

HOSTED BY

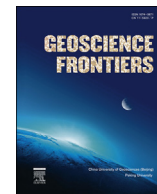


ELSEVIER

Contents lists available at ScienceDirect

China University of Geosciences (Beijing)

Geoscience Frontiers

journal homepage: www.elsevier.com/locate/gsf

Research paper

A primitive mantle source for the Neoproterozoic mafic rocks from the Tanzania Craton

Y.A. Cook^a, I.V. Sanislav^{a,*}, J. Hammerli^a, T.G. Blenkinsop^{a,b}, P.H.G.M. Dirks^a^a Economic Geology Research Centre (EGRU) and Department of Earth and Oceans, James Cook University, Townsville, 4011, QLD, Australia^b School of Earth & Ocean Sciences, Cardiff University, Cardiff CF10 3AT, United Kingdom

ARTICLE INFO

Article history:

Received 14 August 2015

Received in revised form

11 October 2015

Accepted 10 November 2015

Available online 12 December 2015

Keywords:

Mafic rocks

Archean

Tanzania Craton

Primitive mantle

MORB

Oceanic plateau

ABSTRACT

Mafic rocks comprising tholeiitic pillow basalt, dolerite and minor gabbro form the basal stratigraphic unit in the ca. 2.8 to 2.6 Ga Geita Greenstone Belt situated in the NW Tanzania Craton. They outcrop mainly along the southern margin of the belt, and are at least 50 million years older than the supracrustal assemblages against which they have been juxtaposed. Geochemical analyses indicate that parts of the assemblage approach high Mg-tholeiite (more than 8 wt.% MgO). This suite of samples has a restricted compositional range suggesting derivation from a chemically homogenous reservoir. Trace element modeling suggests that the mafic rocks were derived by partial melting within the spinel peridotite field from a source rock with a primitive mantle composition. That is, trace elements maintain primitive mantle ratios ($Zr/Hf = 32–35$, $Ti/Zr = 107–147$), producing flat REE and HFSE profiles [$(La/Yb)_{pm} = 0.9–1.3$], with abundances of 3–10 times primitive mantle and with minor negative anomalies of Nb [$(Nb/La)_{pm} = 0.6–0.8$] and Th [$(Th/La)_{pm} = 0.6–0.9$]. Initial isotope compositions (ϵ_{Nd}) range from 1.6 to 2.9 at 2.8 Ga and plot below the depleted mantle line suggesting derivation from a more enriched source compared to present day MORB mantle. The trace element composition and Nd isotopic ratios are similar to the mafic rocks outcropping ~50 km south. The mafic rocks outcropping in the Geita area were erupted through oceanic crust over a short time period, between ~2830 and ~2820 Ma; are compositionally homogenous, contain little to no associated terrigenous sediments, and their trace element composition and short emplacement time resemble oceanic plateau basalts. They have been interpreted to be derived from a plume head with a primitive mantle composition.

© 2015, China University of Geosciences (Beijing) and Peking University. Production and hosting by Elsevier B.V. This is an open access article under the CC BY-NC-ND license (<http://creativecommons.org/licenses/by-nc-nd/4.0/>).

1. Introduction

Archean greenstone belts include some of the oldest surviving fragments of supracrustal rocks, thus providing important insights into the early evolution of Earth. Some of the oldest greenstone belts include the Isua Greenstone Belt in Greenland (e.g., Myers, 2001; Polat et al., 2002), the Nuvvuagittuq Greenstone Belt in Canada (e.g., O'Neil et al., 2013), the Barberton Greenstone Belt in South Africa (e.g., Cutts et al., 2014) and the Pilbara in Australia (e.g., Green et al., 2000). Moreover, the end of the Archean was a period of widespread volcanism and greenstone belt formation in all major Archean Cratons (e.g., Kerrich et al., 1999; Many and Maboko, 2003; Jayananda et al., 2013; Manikyamba et al., 2014).

The source of this volcanism was attributed to a variety of tectonic processes from subduction settings with the mafic volcanics generated in arcs (e.g., Jayananda et al., 2013; Manikyamba et al., 2014), to plume tectonics with the mafic generated in oceanic plateaus (e.g., Bédard et al., 2014), to a combined process involving both plate tectonics and plumes (e.g., Kerrich et al., 1999). Thus, understanding the geological processes that resulted in greenstone belt formation is essential for understanding crustal growth and evolution through time.

Greenstone belts are integral components of Archean cratons and typically comprise a greenschist to lower amphibolite facies assemblage of complexly interlayered (ultra-)mafic volcanics, sediments and evolved volcanic deposits, which are intruded by igneous bodies and bordered by extensive granites and gneisses. Debate surrounds the types of environment in which Archean greenstone belts formed and hence the tectonic processes that led to development of Earth's early crust, prior to widespread TTG

* Corresponding author. Tel.: +61 07 4781 3293; fax: +61 07 4781 5581.

E-mail address: ioan.sanislav@jcu.edu.au (I.V. Sanislav).

Peer-review under responsibility of China University of Geosciences (Beijing).

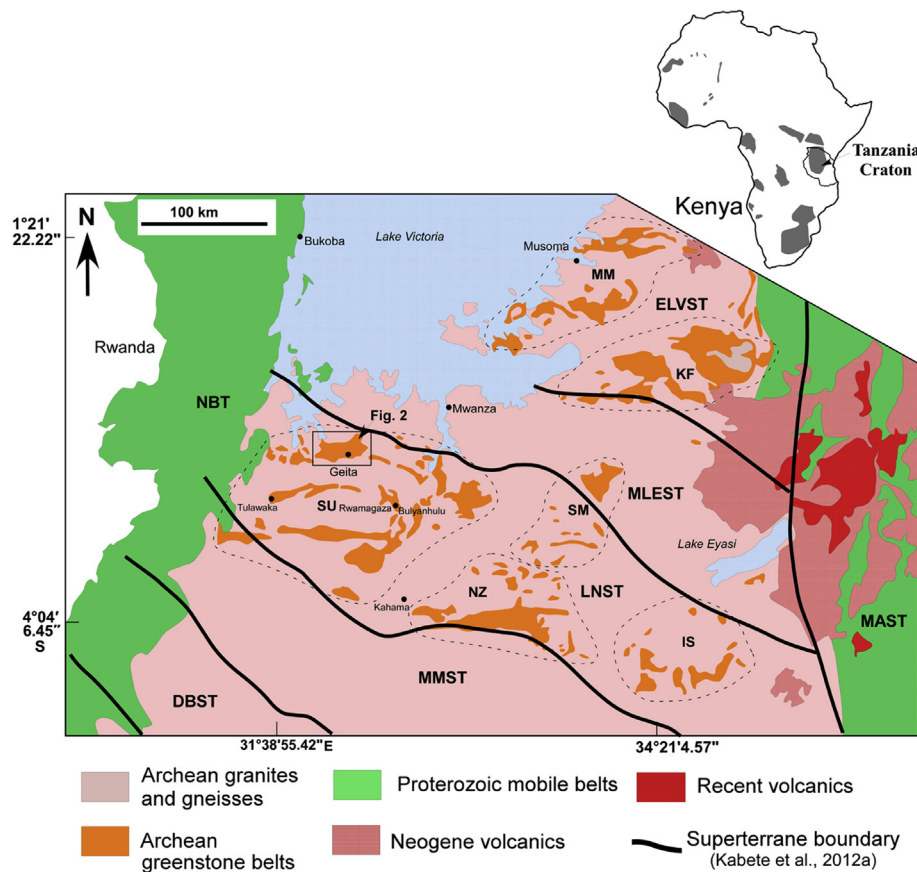


Figure 1. Map of the Tanzania Craton showing the location of the six greenstone belts defined by Borg and Shackelton (1997) and the main tectonic units. SU – Sukumaland Greenstone Belt, SM – Shinyanga-Malita Greenstone Belt, MM – Musoma-Mara Greenstone Belt, KF – Kilimafedha Greenstone Belt, NZ – Nzega Greenstone Belt, IS – Iramba Sekenke Greenstone Belt; Super-terrane boundaries are proposed by Kabete et al. (2012): ELVST – East Lake Victoria, MLEST – Mwanza Lake Eyasi, LNST – Lake Nyanza, MMST – Moyowosi-Manyoni, DBST – Dodoma Basement, MAST – Mbulu-Masai, NBT – Nyakahura-Burigi. Inset map of Africa shows the location of Archean blocks in gray.

intrusion and cratonisation around 2700 Ma (e.g., Condie, 2003; Korenaga, 2006; Van Hunen and Moyen, 2012).

The extensive mafic volcanics and associated rocks that occur commonly in the oldest parts of greenstone belts are central to understanding whether the belts initially formed by eruption of juvenile mantle-derived magmas through older continental crust or in ocean basins and whether they are autochthonous, or incorporated by lateral accretion from an oceanic environment involving subduction-accretion-type processes (e.g., Kuský, 2004; Pearce, 2008; Stott and Mueller, 2009; Bédard et al., 2014).

The volcanic components of greenstone belts commonly show evidence of ocean arc and plateau settings, with or without the influence of plume activity (e.g., Puchtel et al., 1999; Polat and Kerrich, 2000; Parman et al., 2001; Arndt, 2003; Naqvi et al., 2009; Bédard et al., 2014). The high strain zones that occur at the base of volcanic sequences were interpreted to result from lateral accretion of oceanic deposits onto the continent (Kuský and Kidd, 1992; Kuský and Winsky, 1995; Bédard et al., 2014) or as decollements (e.g., Chardon et al., 1996, 1998). Sedimentary and structural data have been used to infer a foreland-type sedimentary basin environment and an allochthonous origin for some greenstone sequences (e.g., Hofmann et al., 2001a, b; Hofmann et al., 2003), and mantle plumes have also been invoked in continental environments (eg., Ohtani et al., 1989; Arndt et al., 1997; Kerrich and Xie, 2002; Arndt, 2003). Evidence for eruption directly onto continental basement includes xenocrysts of lower crustal garnet (Shimizu et al., 2005), crustal geochemical contamination, indicated by changes in the incompatible trace element ratios when

compared to well documented oceanic basalts (Green et al., 2000; Bolhar et al., 2003; Shimizu et al., 2005; Pearce, 2008) and field relations analogous to continental flood basalts such as associated continental sediments (e.g., Choukroune et al., 1995; Hunter et al., 1998; Hollings and Kerrich, 1999; Hollings et al., 1999). It is worth noting that some authors argue that not all greenstone sequences are the same, thus each greenstone belt must be treated independently (e.g., Jelsma and Dirks, 2002). This is particularly well illustrated in the Superior Province where both continental-margin volcanic sequences built on older crustal fragments and juvenile oceanic domains are well documented (e.g., Percival et al., 2006, 2012). In contrast, the greenstone belts of the Tanzania Craton are seriously understudied and there is very limited geological data documenting their stratigraphic, intrusive and deformation histories (e.g., Sanislav et al., 2014). It is generally accepted that the base of the stratigraphy of the greenstone belts from northern Tanzania is formed by mafic volcanics (e.g., Borg, 1992; Manya and Maboko, 2003, 2008) and the available zircon ages (e.g., Sanislav et al., 2014), younger than 2800 Ma, indicate that the mafic volcanics are the oldest rocks in the northern half of Tanzania with no basement rocks identified so far. This may indicate that the mafic volcanics were erupted through oceanic crust thus the potential for crustal contamination is very small.

Mafic volcanic rocks such as basalt represent melt derived from the mantle; therefore, their geochemical composition can provide important insights into the state of the mantle throughout Earth history. For example, modern basalt geochemical composition indicates that the mantle is heterogeneous in composition as a result

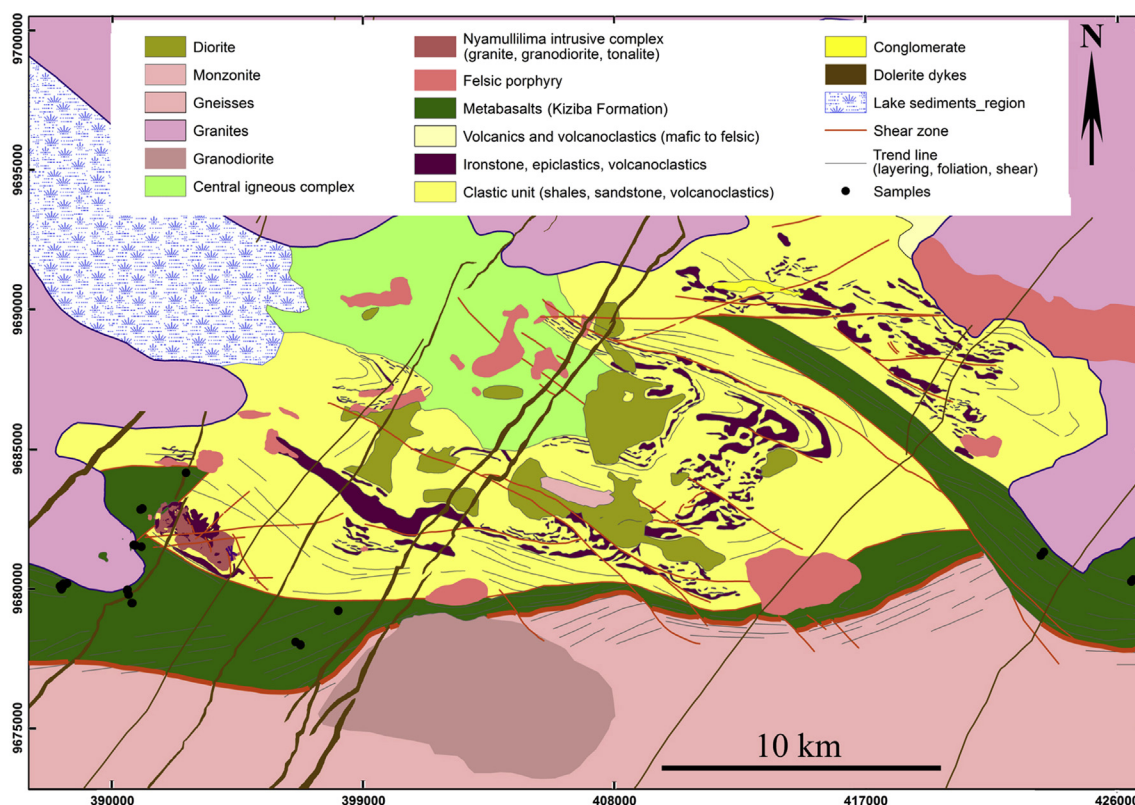


Figure 2. Geological map of the Geita Greenstone Belt showing the main lithological units and the location of samples taken for geochemical analyses used in this study. Coordinates: Arc 1960/UTM zone 36 S.

of the extraction and separation of continental crust through time (e.g., Hofmann, 2003; Williams and Bizimis, 2014; Iwamori and Nakamura, 2015). In general it is accepted that the composition of the mantle from which most modern basalts have been extracted is similar to the composition of modern MORB and OIB (e.g., Pearce, 2008). Many Archean basalts show compositional variations (major and trace elements) that suggest that the Archean mantle had a similar composition to the present day mantle (e.g., Pearce, 2008). If that is the case, then Archean basalt geochemistry may be used to extrapolate present day plate tectonic settings to tectonic interpretations for the Archean and many authors proposed the onset of plate tectonics during the Archean period (e.g., Korenaga, 2013 and references therein). More importantly, Condie (2005) pointed to geochemical evidence indicating that many Archean types of basalt are derived from a mantle source with a primitive mantle composition, and that the state of mantle depletion in the Archean is uncertain. If most of the Archean mantle had a primitive composition it may have serious implications for our understanding of continent evolution and formation. In this contribution we use trace element geochemistry and Nd isotope data from the mafic volcanics that form the base of the greenstone sequences in the northern part of the Tanzania Craton to identify the most likely mantle source composition and their eruptive setting.

2. Regional geology

The Tanzania Craton underlies central and northern Tanzania, south-west Kenya, and south-east Uganda (Clifford, 1970), and is bordered and partly reworked by the Kibaran, Ubendian, Usagaran and Mozambique mobile belts. Granitoid, granitic gneiss, migmatite and high-grade metamorphic supracrustal rocks of the Dodo-man Group comprise the south and central portions of the craton,

bordered to the north by generally lower metamorphic grade granite-greenstone terrains (e.g., Clifford, 1970; Kabete et al., 2012).

In contiguous northwest Tanzania and southwest Kenya eight greenstone belts have been described south and east of Lake Victoria (Fig. 1; Borg and Shackleton, 1997). All these belts have been described in terms of Nyanzian and Kavirondian volcano-sedimentary stratigraphy, and are intruded by a range of syntectonic granitoids of TTG composition prior to further intrusion of high-K granite and crustal consolidation by about 2640 Ma (Barth, 1990; Borg and Shackleton, 1997; Many and Maboko, 2003; Sanislav et al., 2014).

Based on major and trace elements geochemistry of the volcanic rocks, the greenstone belts from the northern half of the Tanzania Craton were interpreted to have formed in accretionary settings reminiscent of modern plate tectonic processes. An immature arc or back-arc environment has been inferred for the Sukumaland Greenstone Belt (Barth, 1990; Many and Maboko, 2003; Many, 2004; Cloutier et al., 2005); a back-arc environment in the Iramba-Sekenke Greenstone Belt (Many and Maboko, 2008) and the southern sector of Musoma-Mara Greenstone Belt; and an island arc environment in the Kilimafedha Greenstone Belt (Wirth et al., 2004; Messo et al., 2012). A continental environment is inferred in the northern sector of Musoma-Mara greenstone belt where plume-influenced subduction is thought to have occurred along a continental margin (Mtoro et al., 2009; Many, 2012).

2.1. The Sukumaland greenstone belt

The Sukumaland Greenstone Belt is exposed in an inferred easterly plunging arcuate structure as two parallel belts of supracrustal rocks, each of which is intruded (and flanked) by granitoid rocks and gneiss (e.g., Quennell et al., 1956; Borg, 1992; Many and Maboko,

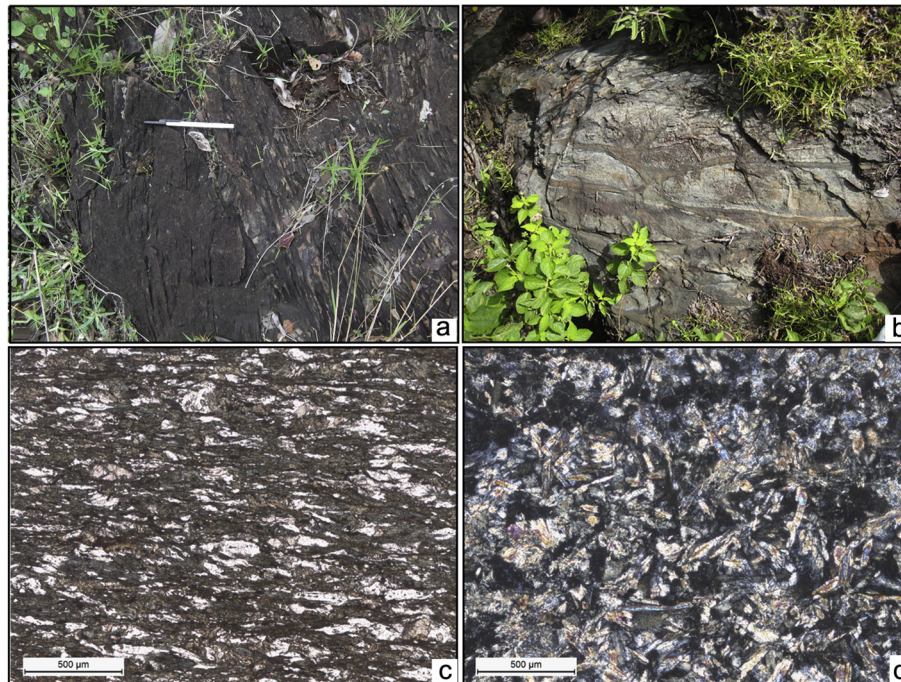


Figure 3. Photographs showing foliated metabasalts (a) and flattened pillow structures (b) from the Kiziba Formation. Photomicrographs showing anastomosing foliation (c) defined by preferential alignment of the hornblende grains from higher strain zones and felty (intergranular) texture (d) found in less deformed basalts from lower strain zones.

2008). The two arcuate belts have commonly been described as two lithologically distinct components of the greenstone belt: (1) the inner belt comprising gabbro and pillow basalt with a generally outward younging direction (Borg, 1992), and with subordinate felsic flows and pyroclastics, all of which have been classified as the lower Nyanzian Supergroup (Quennell et al., 1956; Borg and Shackleton, 1997); and (2) the outer belt comprising iron-rich, carbonaceous and clastic metasedimentary rocks with felsic and intermediate metavolcanic rocks that are classified as part of the upper Nyanzian Supergroup (Barth, 1990; Borg, 1992; Borg and Shackleton, 1997). However, more recent work has indicated that a significant proportion of metasedimentary rocks make up the Tulawaka sector of the inner belt (Cloutier et al., 2005), that mafic volcanic strata are common in the outer belt (e.g., Fawley, 1951; Many and Maboko, 2008), and that young ages occur in the inner belt and old ages in the outer belt (Borg and Krogh, 1999; Many and Maboko, 2003); i.e. there are no distinct lithological and age differences between the two arcuate belts, and the current subdivision of the greenstone belts in northern Tanzania Craton into a lower mafic volcanic dominated unit and upper felsic volcanic and BIF dominated unit may be incorrect (e.g., Many and Maboko, 2008). The mafic volcanic and subvolcanic units described here occur in the Geita sector of the outer arc. Because of the uncertainty with the definition of the Sukumaland Greenstone Belt, we prefer to adopt the terminology of Kuehn et al. (1990) and Sanislav et al. (2014) who use the name Geita Greenstone Belt to refer to this segment of greenstone units.

2.2. The Geita Greenstone Belt

The Geita Greenstone Belt (Fig. 2) is geographically and geologically well defined, incorporating all components found within a typical greenstone belt, including extensive mafic volcanics (e.g., Fawley, 1951; Many and Maboko, 2008; this paper) at the base of the succession followed by an assemblage of cherts, mud rocks, sandstones and ironstones, with felsic to intermediate met-volcanic horizons, which are all intruded by a range of felsic and

intermediate porphyritic bodies (Fig. 2). The Geita Greenstone Belt is sandwiched between undeformed granitic plutons that define its northern margin (Sanislav et al., 2014) and granitoids and gneisses that are in tectonic contact along its southern margin.

Sm and Nd isotope data for mafic volcanics in the southeast of Geita Greenstone Belt show a similar model age (2821 ± 19 Ma; Many and Maboko, 2008) to the 2823 ± 44 Ma (Many and Maboko, 2003) mafic volcanics rocks in the Rwamagaza area of the inner Sukumaland Greenstone Belt, and are the oldest rocks identified in Geita Greenstone Belt. Maximum depositional ages for felsic volcanoclastic and epiclastic deposits are 2771 and 2702 Ma respectively (Chamberlain and Tosdal, 2007), and the minimum age of Geita sedimentation is obtained from a 2699 ± 9 Ma U–Pb zircon age from an intrusive trachyandesite (Borg and Krogh, 1999). Intrusive activity within the belt ranges from 2699 ± 9 to ~ 2620 Ma constraining the timing of tectonic activity in the Geita Greenstone Belt to a period of about 200 Ma (~ 2823 – 2620 Ma; Chamberlain and Tosdal, 2007; Many and Maboko, 2008; Sanislav et al., 2014).

3. Kiziba Formation

The mafic volcanic rocks that outcrop in the Geita and Rwamagaza areas (referred to as the Geita basalts and the Rwamagaza basalts) have near identical geochemical signatures and eruption ages (~ 2820 Ma) and are most probably part of the same eruption event (e.g. Many and Maboko, 2008; this contribution). In this contribution we use the name Kiziba Formation to describe the mafic rocks that outcrop south of Lake Victoria and have similar eruption ages and nearly identical geochemical characteristics. The Kiziba Formation is a package of epidote-amphibolite facies metabasic rocks which form a distinctive lithostratigraphic unit, largely restricted to the southern margin of the Geita Greenstone Belt (Fig. 2). In the west and south of the belt, outcrops of the Kiziba Formation are restricted to several small hills, road cuttings, artisanal mine workings and small scattered outcrops away from hills.

Geological mapping combined with geophysical data (airborne magnetics) confirms that the Kiziba Formation forms a continuous narrow band (Fig. 2) along the southern boundary of the greenstone belt and incorporates the mafic volcanic rocks described by Many and Maboko (2008).

The contacts between the Kiziba Formation and the overlying clastic-volcaniclastic supracrustal association are structural, and locally intruded by late tectonic granitoids. In the west, the lower contact of the formation is juxtaposed with granitic gneiss along an amphibolite facies mylonitic shear zone that marks the southern boundary of the greenstone belt. The upper contact of the formation with adjacent greenschist facies metasedimentary rocks is not exposed, although, in places, exposures of the two lithological units can be found within 10 m of one another. The proximity of the different metamorphic facies (amphibolite facies in the mafic units vs. lower greenschist facies in the metasediment), therefore, necessitates a structural contact. This contact coincides for part of its length with a discrete linear magnetic anomaly corresponding to the contact. The western segment of the upper contact appears to be displaced (Fig. 2) to the north-northeast and is intruded by porphyritic granitoid. In the extreme west-northwest (Fig. 2) of the Geita Greenstone Belt the Kiziba Formation is intruded by extensive undeformed granitoids considered to be correlatives of the high-K, 2660 to 2620 Ma intrusions described by Sanislav et al. (2014) to the north of the Geita Greenstone Belt. The formation extends to the west of Geita Greenstone Belt as a narrow band bordered by granitoids. In the east no contacts are exposed but based on the proximity to the ductile shear zone in the south, the south-eastern contact is considered to be structural while based on the proximity to undeformed granitoids in the north, the north-eastern contact is considered to be intrusive.

The Kiziba Formation comprises basalt, dolerite and minor gabbro with rare fine-grained, amphibole-rich layers that may be metamorphosed tuff. All samples are metamorphosed to the lower amphibolite facies. A variable syn-metamorphic foliation (Fig. 3a–c) is present in most units, locally forming anastomosing high-strain zones that envelop domains of relatively unfoliated rock (Fig. 3d). Although this structural overprint obscures primary relationships, mapping suggests that, in the western portion of the GGB at least, all of the three main rock types (basalt, dolerite and gabbro) are present. Assemblages are dominated by actinolite-hornblende with interstitial oligoclase-andesine and with clinzoisite as a significant accessory mineral, indicating that metamorphism and foliation development occurred under epidote-amphibolite to lower amphibolite facies conditions.

Basalt units are homogeneous, fine-grained and in places have preserved igneous textures (Fig. 3b and d). Individual basalt flows and subvolcanic bodies are locally well preserved, e.g. at the western end of the unit, zones 1–2 m wide contain somewhat preserved pillows (Fig. 3b). The most extensive pillow basalt flow occurs in an elongated zone, 10 m in length and reappears approximately 1.5 km along strike in a smaller band. Pillows up to 60 cm in length and 30 cm in width contain 1 cm wide rims and mineral-filled vesicles (quartz and carbonate) up to 4 mm in diameter. Concentration of vesicles along one edge of the pillows indicates younging to the north.

Gabbro units represent the most feldspar-rich and texturally variable rock type in the Kiziba Formation. Some contain relict olivine cores surrounded by pyroxene with interstitial plagioclase, with hornblende locally forming pseudomorphs after pyroxene, and, rarely, gabbro contains late-stage igneous quartz and apatite. Clinzoisite is accessory, some of which replaces amphibole; and plagioclase and olivine are commonly altered to sericite, and carbonate respectively.

Table 1
The major element composition (in wt.%) for the Kiziba Formation metabasalts.

Sample	E1	E4	E5	E6	IH11	IH12	IH8	IH9	K43	K45	K56	K73	K75	K76	K82	K83	K84	KH14	KH15	KH18	KH2	KH3	KH4	KH7	LH8
SiO ₂	48.71	49.08	53.69	51.64	48.43	49.62	48.71	48.15	48.73	48.95	48.33	49.39	52	49.43	49.65	48.9	48.05	48.16	48.54	48.63	47.97	52.94	54.86	48.65	47.59
TiO ₂	1.12	1.18	0.89	1.03	1.18	1.1	1.26	1.09	1.07	0.65	1.4	1.2	1.7	1.19	1.06	1.04	1.15	1.32	1.25	1.32	1.14	1.36	1.17	1.23	0.71
Al ₂ O ₃	14.54	14.05	14.51	14.07	13.48	13.81	13.27	14.5	13.09	13.13	13.67	14.4	11.97	14.75	14.74	14.48	15.04	14.73	13.69	15.76	14.48	13.14	13.85	13.45	14.33
FeO	14.79	14.34	8.93	12.7	14.48	13.47	15.7	14.07	15.22	12.84	16.38	14.53	15.91	12.49	13.87	13.86	15.56	14.6	14.55	14.41	14.43	13.45	11.51	15.37	12.36
MnO	0.22	0.21	0.21	0.25	0.22	0.22	0.23	0.21	0.24	0.18	0.21	0.23	0.26	0.21	0.2	0.22	0.22	0.2	0.19	0.22	0.23	0.21	0.19	0.22	0.19
MgO	7.56	7	6.69	5.35	7.11	7.73	6.74	6.81	6.07	9.06	6.24	7.31	5.53	6.22	7.11	6.93	6.67	7.02	7.35	6.58	7.76	6.29	4.8	6.65	8.42
CaO	9.47	9.95	9.97	12.68	10.3	10.06	9.3	9.57	8.31	12.33	7.47	8.81	9.79	11.36	8.76	10.53	10.92	9.35	8.32	9.28	9.27	9.21	10.53	8.7	10.61
Na ₂ O	2.56	2.09	3.49	1.32	2.94	2.52	2.83	2.78	2.73	1.74	4.02	3.15	0.91	2.09	3.55	2.73	2.3	3.01	3.37	3.31	2.13	3.74	2.91	3.64	2.23
K ₂ O	0.42	0.32	0.14	0.12	0.14	0.42	0.18	0.16	0.14	0.21	0.21	0.21	0.23	0.09	0.22	0.31	0.18	0.14	0.08	0.1	0.9	0.42	0.14	0.29	0.5
P ₂ O ₅	0.1	0.11	0.1	0.12	0.12	0.1	0.11	0.1	0.11	0.07	0.13	0.11	0.15	0.12	0.1	0.11	0.13	0.12	0.12	0.14	0.12	0.13	0.11	0.11	0.07
Total	99.49	98.33	98.62	99.28	98.4	99.04	98.33	97.44	95.71	99.16	98.06	99.36	98.31	98.15	99.26	99.11	100.22	98.65	97.46	99.75	98.43	100.89	100.07	98.31	97.01

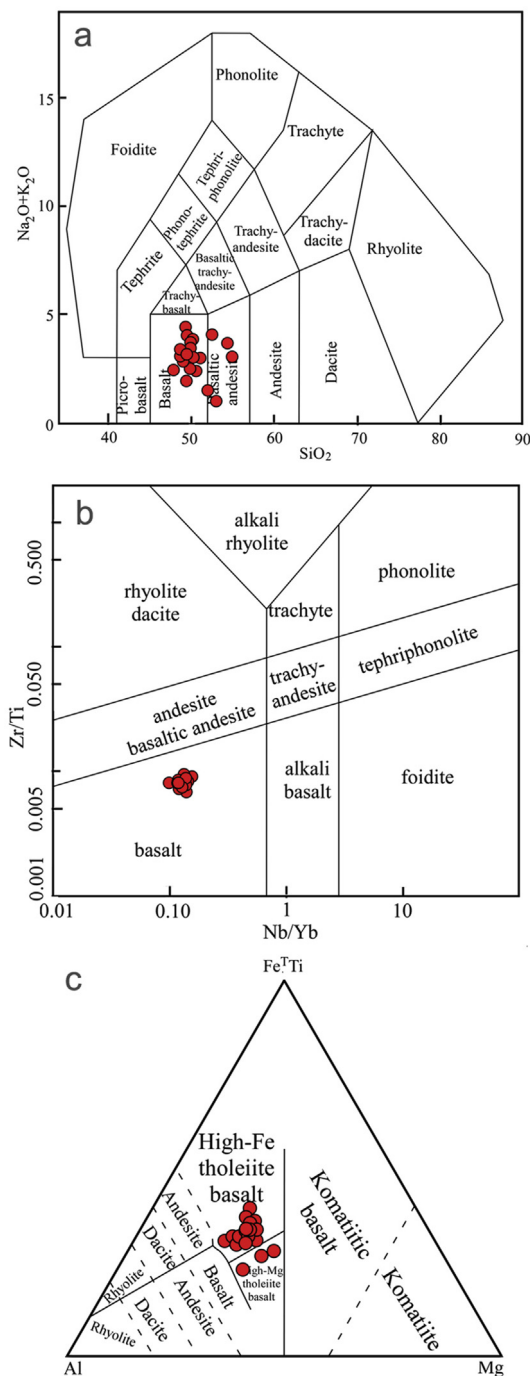


Figure 4. Major elements (a) and trace elements (b) classification diagrams for Kiziba Formation metabasalts. (c) Discrimination diagram showing that Kiziba Formation metabasalts are high-Fe tholeiites.

Millimeter scale veining is developed locally in all rock types and comprises varying amounts of biotite, quartz, clinozoisite and lesser pyrrhotite, calcite, pyrite, pentlandite, chalcopyrite, sphalerite and ilmenite.

4. Geochemistry

Twenty-five samples of the least altered mafic units were collected from different outcrops across the Kiziba Formation

(Fig. 2). They were analyzed for major and trace element concentrations. Eight samples from the western part of the GGB were analyzed for Sm and Nd isotopes. Some samples host minor epidote-calcite veining or are silicified, but interpretation of elements considered relatively immobile, including Al, Ti, high-field-strength elements (HFSE) and rare-earth elements (REE) allows inclusion of silicified samples for analysis (e.g., Arndt and Nesbitt, 1982; Jochum et al., 1991; Laflèche et al., 1992).

4.1. Analytical methods

For whole rock geochemical analyses representative sample material was milled to a fine powder in a tungsten carbide ring mill at James Cook University (JCU). Major elements were analyzed at the Advanced Analytical Centre (JCU), by conventional X-ray fluorescence (XRF) using a Bruker-AXS S4 Pioneer XRF Spectrometer on fused beads. The fused beads consist of rock powders mixed with 12:22 borate flux (Lithium Tetraborate 35.3%/Lithium Metaborate 64.7%; XRF Scientific Limited, Perth, Australia) at 1:8 sample to flux ratio that were fused to glass after heating to 1050 °C for 15 min in a F-M 4 Fusion Bead Casting Machine (Willunga, Australia). For further trace element analyses, chips of the fused beads were mounted into a standard epoxy puck and analyzed for a range of trace elements using a Geolas Pro 193 nm ArF Excimer laser ablation unit (Coherent) coupled to Varian 820 quadrupole ICP-MS. Helium was used as the carrier gas (0.8 L/min), which was subsequently mixed with Ar via a mixing bulb between the ablation cell and the ICP-MS to smooth the ablation signal. Laser energy density was set to 6 J/cm², and laser spot size and repetition rate were set to 120 μm and 10 Hz, respectively. Each fused bead was analyzed 3 times and average values are reported. The ICP-MS was tuned to ensure robust plasma conditions (sensitivity of Th ≈ U ≈ Pb; e.g., Pettke, 2008) and low oxide production levels (≤0.5% ThO) with the plasma power set at 1.25 kW. NIST SRM 610 glass was used as a bracketed external standard using the standard reference values of Spandler et al. (2011). Data were quantified using Ca (as previously determined by XRF on the same fused bead) as the internal standard, and data were processed using the Glitter software (Van Achterbergh et al., 2001). In order to monitor precision and accuracy of the analyses, we analyzed Hawaiian basalt reference glass (KL2-glass; n = 21) as a secondary standard (Jochum et al., 2006). The precision for REE analyses by LA-ICP-MS is better than 5% (mostly <3%), and the accuracy is better than 6%, often <2%. Cesium, Rb and Cu showed the lowest accuracies compared to KL2-glass (12%, 14% and 19%). However, these relatively large uncertainties might be related to the considerable uncertainties of concentrations in the KL2-glass (see appendix for details Table A-1 and Spandler et al., 2011 for comparison). The standard reference material NIST612 (n = 11) was analyzed as a ternary standard. The precision for all the elements, besides Zn (3.5%) and Ge (~8.3%) is <2%, and <1% for REE. The accuracy for all the elements (standard reference concentrations taken from Spandler et al., 2011) is <3%. The only exceptions are Tb (6.5%), Ge (~8.3%), Sb (~9%), and Zn (~5.3%) where relatively large uncertainties in the NIST612 glass have to be taken into consideration. Typical detection limits for REE are in the ppb-range and are given in Table A-1.

Neodymium and samarium isotope analyses were performed at University of Adelaide on a Finnegan MAT262 thermal ionization mass spectrometer. The mass spectrometer measurement uncertainty in the (spiked) ¹⁴³Nd/¹⁴⁴Nd for BCR-2 is 0.512678 ± 0.000009 (2SE). The long term external lab precision on BHVO-2 for ¹⁴³Nd/¹⁴⁴Nd ratio is 0.002% (SD) and for ¹⁴⁷Sm/¹⁴⁴Nd is 0.3% (SD). The reference values used in ε_{Nd} calculations are (¹⁴³Nd/¹⁴⁴Nd)_{CHUR} = 0.512638, (¹⁴⁷Sm/¹⁴⁴Nd)_{CHUR} = 0.1966 and λ = 6.54 × 10⁻¹² a⁻¹.

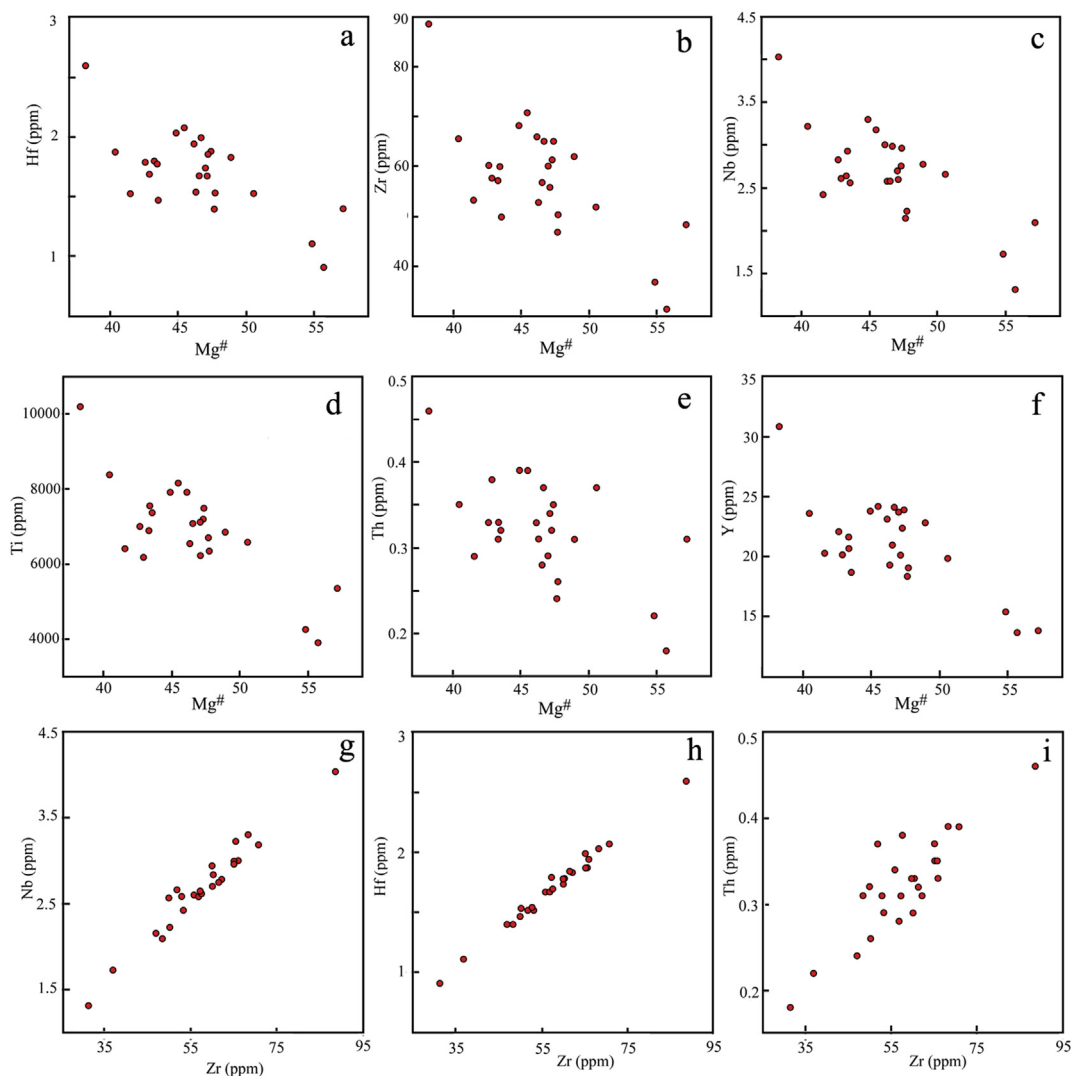


Figure 5. Element variation diagram showing the relationship between $Mg^{\#}$ and selected trace elements (a–f) and the linear relationship between Zr and HFSE (g–i).

4.2. Major and trace elements geochemistry

The metabasalt units in the Kiziba Formation have SiO_2 values (Table 1) below 50 wt.% (47.59–49.65 wt.%) except 5 samples that were slightly silicified (micro-quartz veins) and thus have higher SiO_2 (51.64–57.86 wt.%). The silicification makes these samples fall into the basaltic andesite field on a TAS classification diagram (Fig. 4a). However based on their trace elements all samples cluster tightly into the basalt field (Fig. 4b). All samples have low alkali content and, thus, classify as tholeiitic basalt (Fig. 4c). Most samples fall into the field of high-Fe tholeiitic basalt except three samples that have low FeO (sample E5) and TiO_2 (samples K45 and LH8), which makes them high-Mg tholeiite basalt. Overall, the $Mg^{\#}$ varies between 36 and 57 indicating they are moderately- to well-evolved basalts, corresponding to the transition from magnesian tholeiite ($Mg^{\#} = 57$) to Fe-rich tholeiite ($Mg^{\#} = 36$). The concentration of selected immobile elements shows an inverse relationship when plotted (Fig. 5a–f) against magnesium numbers indicating clear fractionation trends from the least to the most evolved samples. There is also a direct correlation between Zr and other HFSE (Fig. 5g–i), suggesting that the HFSE concentrations were not

disturbed during subsequent deformation and metamorphism. However, the Kiziba Formation metabasalts are not primary melts and are moderately to strongly evolved as indicated by their low $Mg^{\#}$ (0.57–0.38), and have experienced fractionation prior to emplacement. Herzberg and Asimov (2008) have shown that mafic primary magmas first fractionate olivine followed by pyroxene and plagioclase (Fig. 6a). Once pyroxene and plagioclase start crystallizing, the CaO content of the melt will decrease rapidly as exemplified by the continuous line in Fig. 6a. All samples plot near this line suggesting that the Kiziba Formation metabasalts have experienced olivine + pyroxene + plagioclase fractionation.

The Kiziba Formation basalts have a flat chondrite-normalized REE pattern (Fig. 6b; Table 2) and show a small negative to positive Eu anomaly ($Eu/Eu^* = 0.86–1.06$) indicating minor plagioclase fractionation. In some samples LREE are slightly depleted [$(La/Sm)_{cn} = 0.81–1.22$; $cn =$ chondrite normalized] compared to HREE [$(Gd/Yb)_{cn} = 1.11–1.29$]. When normalized to primitive mantle (Fig. 6c) REE profiles are flat [$(La/Yb)_{pm} = 0.9–1.3$; $pm =$ primitive mantle normalized]. There is a small negative anomaly of Nb [$(Nb/La)_{pm} = 0.56–0.81$] and Th [$(Th/La)_{pm} = 0.55–0.93$], but the overall pattern is flat with 3–10 times primitive mantle values.

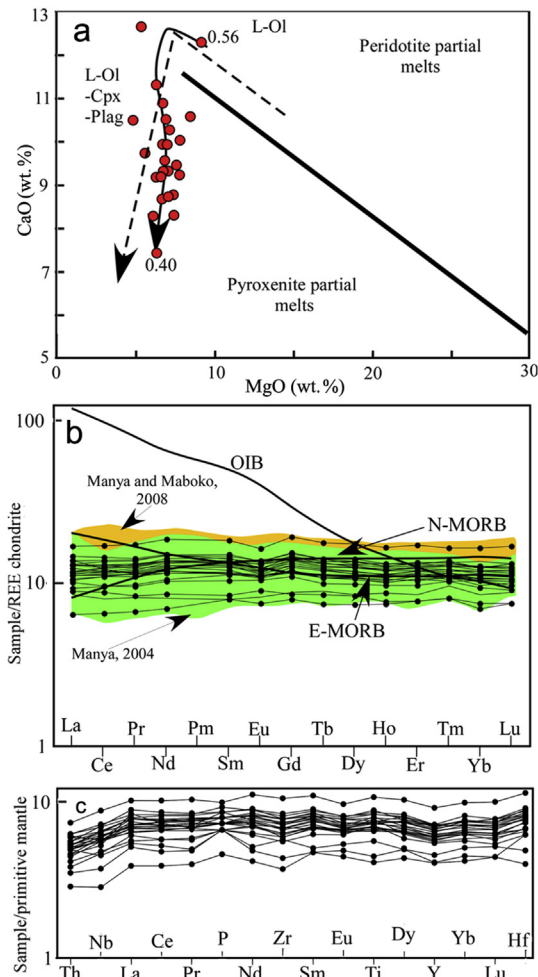


Figure 6. Diagrams showing (a) CaO versus MgO content on Kiziba Formation metabasalts plotted on the [Herzberg and Asimov \(2008\)](#) diagram showing the effect of olivine, clinopyroxene and plagioclase fractionation on a fertile peridotite, and the REE (b) chondrite normalized pattern ([Sun and McDonough, 1989](#)) and selected immobile trace elements (c) normalized to primitive mantle values of [Lyubetskaya and Korenaga \(2007\)](#).

4.3. Nd-isotopic data

Neodymium isotopic data for eight samples from Kiziba Formation basalt are presented in [Table 3](#). The $^{147}\text{Sm}/^{144}\text{Nd}$ ratios range from 0.186 to 0.198, and the $^{143}\text{Nd}/^{144}\text{Nd}$ ratios range from 0.51257 to 0.51281. They have a similar initial ϵ_{Nd} (at 2800 Ma) with values between 1.65 and 2.94 epsilon units. The average ϵ_{Nd} at 2800 Ma for all samples is 2.4 ± 0.4 and the lack of any correlation between $^{143}\text{Nd}/^{144}\text{Nd}$ ratio and Nd concentration suggests very small to no isotopic contamination by preexisting felsic crust. Most likely the isotope data can be explained by small degree of mixing of two mantle sources. Positive ϵ_{Nd} in oceanic plateaus such as the Ontong Java Plateau has been explained in terms of mixing/interaction of a deep primitive mantle source with the depleted upper mantle (e.g. [Kerr and Mahoney, 2007](#)). A plot of $^{143}\text{Nd}/^{144}\text{Nd}$ vs. $^{147}\text{Sm}/^{144}\text{Nd}$ for Kiziba basalt produced a poorly defined Sm–Nd errorchron with an imprecise age of 3132 ± 490 Ma. The isochron is poorly defined due to the restricted range in the $^{147}\text{Sm}/^{144}\text{Nd}$ and $^{143}\text{Nd}/^{144}\text{Nd}$ ratios ([Table 2](#)). However, when combining our dataset with data presented in [Manya and Maboko \(2008\)](#) a more precise age can be derived of 2819 ± 18 Ma ([Fig. 7](#)), thus, confirming the earlier interpretation that metabasalt in the Geita Greenstone Belt erupted at ~ 2800 Ma ([Manya and Maboko, 2008](#)).

5. Fractionation and partial melting

Harker variation diagrams ([Fig. 5](#)) illustrate systematic behavior, and indicate that there has been some differentiation during evolution of the formation, but that magma chamber contamination and mixing were not significant processes, and that there has been little secondary mobility of REE's or HFSE's. Selected element ratios are likely to approximate those of the original melts; in particular Zr and Hf are not fractionated from each other, with Zr/Hf ratios (31.98–35.09) close to the primitive mantle value of 36 ([Sun and McDonough, 1989](#)), and Ti/Zr ratios are consistent (Ti/Zr = 107–147) and similar to primitive mantle ratios of 116 ([Sun and McDonough, 1989](#)). The absence of a negative Ti anomaly [$(\text{Dy}/\text{Ti})_{\text{pm}} = 0.82\text{--}1.15$] suggests that no Ti-bearing mineral phase was involved in fractionation.

6. Depth and temperature of melting

The Kiziba Formation basalt samples cluster at 14.04% Al_2O_3 and 0.70 for $\text{CaO}/\text{Al}_2\text{O}_3$ ratio, which is consistent with segregation of primary magmas at 2–3 GPa ([Fig. 8a](#); [Herzberg, 1995](#)). Most of the samples plot to the left of the solidus, suggesting that none of the basalts that were sampled are primary magmas. One mechanism for reducing $\text{CaO}/\text{Al}_2\text{O}_3$ and causing a shift to the left of the solidus is fractionation of clinopyroxene or by a source region that was inherently low in $\text{CaO}/\text{Al}_2\text{O}_3$ (e.g., [Herzberg, 1995](#)). We interpret the positioning of most samples to the left of the solidus as a consequence of pyroxene and plagioclase fractionation and not a reflection of the source region composition. The average pressure and temperature of melting calculated with the method described by [Till et al. \(2012\)](#) is 2.2 GPa and 1405 °C, which corresponds to an approximate depth of 60–70 km, in good agreement with the results obtained by using the [Herzberg \(1995\)](#) method. This temperature and pressure range suggests that Kiziba Formation metabasalt was generated at pressures higher than most of the present day MORB from the Atlantic and Pacific, but at similar temperature ranges ([Fig. 8b](#)). [Fig. 8b](#) also suggests the metabasalt was generated by $\sim 10\%$ melting near the spinel-garnet transition zone. Modeling of spinel lherzolite and garnet lherzolite melting ([Fig. 9](#)) indicates that most probably the metabasalt units in the Kiziba Formation are spinel lherzolite melts derived from a primitive mantle source. The best approximation is given by non-modal batch melting ([Fig. 9a](#)) with melt fractions between 0.1 and 0.2. Non-modal fractional melting ([Fig. 9b](#)) cannot explain the observed element ratios while continuous melting ([Fig. 9c](#)) can reproduce the observed element ratios for very small melt fractions (0.03–0.1).

7. LREE enrichment/depletion and negative Eu anomaly

The REE pattern of Kiziba Formation metabasalt is characterized by an overall flat pattern and a small negative Eu anomaly ([Fig. 6a](#)). The overall flat appearance of the REE pattern is given by a combination of samples having LREE depleted or enriched with $(\text{La}/\text{Yb})_{\text{CN}}$ ranging between 0.90 and 1.30. Different degrees of melting of a source material with a primitive mantle composition can produce the observed pattern in REE distribution ([Fig. 10](#)). Non-modal batch melting ([Fig. 10a](#)) of a primitive mantle source can produce the observed LREE enrichment/depletion for melt fractions between 0.2 and 0.1. Non-modal fractional melting can produce the same effect at very low melt fractions ([Fig. 10b](#)) while continuous melting can produce the observed effect for melt fractions between 0.1 and 0.01 ([Fig. 10c](#)). [Fig. 10](#) also shows the effect of partial melting on the Eu anomaly. It is worth noting that non-modal batch melting will produce only negative Eu anomalies ([Fig. 10a](#)) for melt fractions

Table 2

The trace element composition (in ppm) and the selected element ratio for the Kiziba Formation metabasalts.

Sample	E1	E4	E5	E6	IH11	IH12	IH8	IH9	K43	K45	K56	K73	K75	K76	K82	K83	K84	KH14	KH15	KH18	KH2	KH3	KH4	KH7	LH8
Sc	36.38	40.29	42.39	40.65	47.35	40.33	40.7	40.74	38.12	47.24	43.45	42.68	41.25	42.75	39.06	42.1	39.12	42.03	40.94	44.52	39.67	37.98	39.22	37.53	46.82
V	327.45	327.07	281.24	292.49	339.08	303.13	348.23	307.22	295.8	263.11	363.97	335.76	388.2	350.02	305.22	302.81	312.34	345.33	332.81	354.48	324.24	336.64	314.37	321.4	272.83
Cr	133.79	158.53	159.91	117.21	240.6	82.4	108.24	202.1	34.36	178.39	112.81	201.04	82.95	162.98	185.29	212.25	178.62	178.58	166.98	181.37	166.36	132.81	169.29	121.37	185.11
Cu	94.16	94.06	85.75	117.87	88.64	20.72	108.96	105.94	103.42	175.32	113.78	83.89	75.12	99.44	101.64	108.74	97.43	104.92	79.9	103.29	69.35	97.27	50.95	86.41	138.53
Zn	67.41	73.04	55.29	68.08	80.05	59.35	87.68	78.44	68.16	54.67	68.23	73.84	80.21	80.1	66.38	86.42	77.9	77.09	69.75	82.31	66.45	71.19	60.85	85.28	66.34
Ga	14.42	14.63	13.62	14.23	18.49	12.18	14.3	13.95	14	11.7	14.98	14.71	14.55	15.63	13.93	14.25	15.15	16.17	13.29	15.82	14.94	12.39	11.82	13.41	13.57
Ge	1.73	1.72	1.91	1.65	2.02	1.67	2.01	1.53	1.33	1.9	1.54	1.81	1.97	1.26	1.43	1.48	2.25	2.13	1.25	1.81	1.61	1.8	1.64	2.42	1.91
As	5.04	1.96	7.66	15.03	3.06	1.56	1.35	1.89	1.3	1.21	2.37	12.2	4.08	10.1	4.37	7.38	8.53	7.74	1.03	3.75	21.97	14.88	30.33	5.29	21.4
Rb	22.33	13.16	4.07	4.41	2.79	17.23	1.33	2.37	3.84	4	5.37	4.97	4.78	12.61	8.57	6.59	3.29	3.6	1.28	3.92	46.5	16.81	2.9	7.89	26.01
Sr	148.74	107.55	196.22	99.46	68.66	129.42	90.52	105.03	105.68	96.34	111.85	108.8	125.19	124.85	124.88	76.28	98.27	96.08	65.88	131.27	131.6	147.41	117.17	147.6	191.97
Y	18.36	21.01	13.84	20.18	24.1	19.85	21.68	19.37	20.32	13.72	23.57	22.42	30.87	23.75	19.03	20.15	20.66	23.11	23.86	23.82	22.81	24.14	22.12	18.71	15.4
Zr	46.96	56.83	48.37	57.59	65.15	51.8	59.98	52.83	53.25	31.31	65.55	61.37	88.7	60.06	50.24	55.86	57.25	65.92	65.16	68.32	62.13	70.82	60.26	49.97	36.78
Nb	2.15	2.57	2.09	2.61	2.98	2.66	2.93	2.58	2.42	1.31	3.22	2.75	4.04	2.7	2.22	2.6	2.64	3	2.96	3.3	2.78	3.18	2.83	2.56	1.72
Mo	1.12	0.95	1.06	1.42	1.36	0.84	1.26	1.04	1.47	1.23	0.91	0.98	1.4	1.37	1.01	1.07	1.38	1.19	0.91	0.83	1.06	1.1	1.03	1.13	1.08
Sn	1	1.29	0.92	1.2	1.18	0.87	1.05	0.99	1.04	1.07	1.11	1.17	1.21	1.44	0.9	1.09	1.21	1.28	1.4	1.22	1.21	1.12	1.12	1.15	1.38
Sb	0.78	0.69	0.91	1.36	0.74	0.85	0.61	0.47	0.45	0.64	1.03	1.13	1.41	3.65	0.74	1.81	2.15	0.81	0.63	1.15	1.1	0.81	1.26	0.64	1.17
Cs	0.77	1	1.45	1.54	0.55	5.18	0.46	0.67	0.32	0.42	2.64	0.61	0.63	1.91	1.02	2.89	1.37	1.5	0.84	2.03	1.7	1.04	0.3	2.25	1.88
Ba	197.75	64.85	81.54	40.28	24.32	50.08	36.24	42.84	32.24	35.7	44.21	41.87	51.95	38.93	39.75	45.8	30.21	35.51	23.14	62.35	141.82	96.68	58.22	101.01	40.89
La	3.1	3.28	2.76	3.79	3.98	3.23	3.97	3.43	4.27	1.98	4.52	3.54	5.18	3.95	2.86	3.62	3.44	3.95	3.64	4.21	3.6	4.02	3.48	3.45	2.62
Ce	7.72	8.82	7.03	9.5	10.19	8.78	10.41	8.97	9.79	5.23	11.52	9.34	13.66	10.08	7.69	9.6	9.21	10.38	9.99	11.11	9.89	10.94	9.48	9	6.44
Pr	1.16	1.39	1.01	1.4	1.56	1.33	1.55	1.37	1.38	0.81	1.72	1.46	2.1	1.53	1.19	1.41	1.43	1.6	1.58	1.69	1.52	1.66	1.49	1.38	0.99
Nd	6.12	7.33	5.13	7.11	8.43	6.87	8.19	7.02	6.88	4.15	8.98	7.89	11.07	8.2	6.27	7.45	7.59	8.2	8.2	8.77	8.04	8.88	7.64	7.13	4.84
Sm	2.01	2.42	1.64	2.19	2.76	2.25	2.65	2.26	2.21	1.54	2.72	2.64	3.55	2.54	2.18	2.33	2.47	2.6	2.65	2.84	2.57	2.91	2.51	2.22	1.54
Eu	0.76	0.86	0.66	0.8	0.9	0.82	0.87	0.81	0.78	0.55	0.98	0.95	1.19	0.86	0.81	0.79	0.83	0.96	0.95	1	0.9	0.99	0.84	0.81	0.6
Gd	2.82	3.29	2.2	3.08	3.72	3.04	3.4	3.02	3.04	2.05	3.73	3.59	4.95	3.6	3.03	3.22	3.29	3.78	3.64	3.88	3.56	3.96	3.54	2.97	2.26
Tb	0.47	0.57	0.4	0.51	0.64	0.52	0.58	0.51	0.53	0.35	0.62	0.63	0.83	0.6	0.51	0.56	0.57	0.64	0.66	0.66	0.62	0.66	0.59	0.51	0.42
Dy	3.15	3.64	2.68	3.47	4.35	3.48	3.79	3.45	3.53	2.36	4.15	4.02	5.56	4.02	3.42	3.65	3.76	4.31	4.17	4.35	4.09	4.48	3.98	3.36	2.73
Ho	0.69	0.8	0.55	0.74	0.93	0.74	0.8	0.72	0.77	0.53	0.89	0.87	1.18	0.86	0.76	0.77	0.81	0.91	0.94	0.9	0.85	0.94	0.85	0.72	0.62
Er	2.02	2.39	1.62	2.3	2.79	2.31	2.48	2.22	2.34	1.62	2.66	2.6	3.56	2.58	2.17	2.39	2.46	2.75	2.72	2.8	2.64	2.78	2.48	2.21	1.77
Tm	0.33	0.36	0.26	0.36	0.43	0.37	0.38	0.33	0.34	0.26	0.42	0.41	0.53	0.39	0.35	0.36	0.37	0.41	0.44	0.43	0.41	0.43	0.39	0.35	0.31
Yb	1.95	2.23	1.56	2.15	2.56	2.21	2.45	2.15	2.24	1.45	2.64	2.59	3.42	2.45	2.16	2.2	2.29	2.65	2.57	2.6	2.5	2.82	2.37	2.02	1.76
Lu	0.29	0.34	0.24	0.33	0.42	0.34	0.37	0.31	0.34	0.24	0.4	0.39	0.54	0.38	0.33	0.34	0.36	0.4	0.42	0.4	0.38	0.42	0.36	0.32	0.28
Hf	1.4	1.67	1.4	1.69	1.99	1.52	1.78	1.54	1.52	0.91	1.87	1.84	2.59	1.74	1.53	1.67	1.79	1.94	1.87	2.03	1.83	2.07	1.78	1.47	1.11
Pb	1.37	0.97	2.06	2.01	1.43	1.5	1.07	1.29	0.81	0.98	1.57	6.32	2.84	5.87	3.04	4.1	2.07	2.63	1.36	2.14	3.45	1.35	1.83	2.08	3.59
Th	0.24	0.28	0.31	0.38	0.37	0.37	0.33	0.31	0.29	0.18	0.35	0.32	0.46	0.29	0.26	0.34	0.31	0.33	0.35	0.39	0.31	0.39	0.33	0.32	0.22
U	0.06	0.07	0.08	0.09	0.12	0.09	0.09	0.07	0.07	0.13	0.09	0.08	0.13	0.08	0.07	0.09	0.08	0.09	0.1	0.1	0.08	0.11	0.08	0.08	0.07
Mg [#]	0.48	0.47	0.57	0.43	0.47	0.51	0.43	0.46	0.42	0.56	0.40	0.47	0.38	0.47	0.48	0.47	0.43	0.46	0.47	0.45	0.49	0.45	0.43	0.44	0.55
Eu/Eu*	0.97	0.93	1.06	0.94	0.86	0.96	0.88	0.95	0.92	0.94	0.94	0.94	0.87	0.87	0.96	0.88	0.89	0.93	0.93	0.92	0.91	0.89	0.86	0.96	0.98
Zr/Hf	33.54	34.03	34.55	34.08	32.74	34.08	33.70	34.31	35.03	34.41	35.05	33.35	34.25	34.52	32.84	33.45	31.98	33.98	34.84	33.66	33.95	34.21	33.85	33.99	33.14
Ti/Zr	142.98	124.48	110.31	107.22	108.58	127.31	125.94	123.69	120.46	124.46	128.04	117.23	114.90	118.78	126.49	111.62	120.43	120.05	115.01	115.83	110.00	115.13	116.40	147.57	115.73
Th/Ce	0.03	0.03	0.04	0.04	0.04	0.04	0.03	0.03	0.03	0.03	0.03	0.03	0.03	0.03	0.03	0.04	0.03	0.03	0.04	0.04	0.03	0.04	0.03	0.04	0.03
Nb/Th	8.96	9.18	6.74	6.87	8.05	7.19	8.88	8.32	8.34	7.28	9.20	8.59	8.78	9.31	8.54	7.65	8.52	9.09	8.46	8.46	8.97	8.15	8.58	8.00	7.82

Table 3
The Nd isotope composition for the Kiziba Formation metabasalts.

Sample	Age of rock <i>T</i> (Ma)	Unmixed $^{143}\text{Nd}/^{144}\text{Nd}$	Nd ($\mu\text{g/g}$)	Sm ($\mu\text{g/g}$)	$^{147}\text{Sm}/^{144}\text{Nd}$	$\epsilon_{\text{Nd}}(T=0)$	$^{143}\text{Nd}/^{144}\text{Nd}(T)$	$\epsilon_{\text{Nd}}(T)$	T_{DM} (Ma)	DM at age of rock (<i>T</i>)
IH8	2800	0.512577	14.79004	4.582894	0.187343	−1.18	0.509115	2.17	3190	0.509186
IH11	2800	0.512751	10.01173	3.222589	0.194609	2.21	0.509155	2.94	3037	0.509186
K56	2800	0.512582	12.75315	3.930219	0.186323	−1.09	0.509139	2.64	3050	0.509186
K83	2800	0.512596	8.327947	2.602303	0.188924	−0.81	0.509105	1.97	3275	0.509186
K84	2800	0.512693	9.042236	2.90105	0.193976	1.07	0.509108	2.03	3367	0.509186
KH3	2800	0.512684	9.848717	3.111574	0.191015	0.89	0.509154	2.93	3006	0.509186
K82	2800	0.512789	7.131534	2.337014	0.198128	2.94	0.509127	2.41	3337	0.509186
KH14	2800	0.512701	10.92093	3.484267	0.192894	1.24	0.509137	2.59	3142	0.509186

less than 0.3, fractional melting will produce negative Eu anomalies only at very low melt fractions, while continuous melting will produce positive Eu anomalies for melt fractions equal or higher than 0.15 and negative Eu anomalies for melt fractions less than 0.15. Plagioclase fractionation, which is indicated by the relationship shown in Fig. 6a and by constant Al_2O_3 is the most likely cause for the negative Eu anomaly.

8. Crustal and/or subduction related contamination

The Kiziba Formation metabasalts are the oldest rocks in the Lake Victoria region (e.g., Many and Maboko, 2008; Sanislav et al., 2014); they contain pillow structures and rare intercalations of hydrothermal chert and/or thin black shale horizons, and most probably represent oceanic basalt flows (e.g., Many and Maboko, 2008). Certain incompatible and immobile element ratios can be used to track crustal contamination/interaction of/basaltic magmas. La/Nb ratio (Condie, 2003) can be used to identify a possible subduction/crustal contamination component in which basalt with La/Nb > 1.4 is interpreted to reflect subduction and/or crustal contamination of the source magmas. The La/Nb ratio for Kiziba Formation metabasalts varies from 1.21 to 1.76 with an average of 1.36, suggesting that some samples may have experienced some form of subduction and/or crustal contamination. Crustally contaminated Archean basalts from the Superior Province typically have $(\text{La}/\text{Sm})_{\text{cn}}$ ratios of >1.5 and Th/Ce ratios >0.05 (Kerrick et al., 1999). The samples from the Geita Greenstone Belt have $(\text{La}/\text{Sm})_{\text{cn}}$ ratios between 0.8 and 1.21 with an average of 0.94 and Th/Ce < 0.05. Another filter used to identify samples with crustal contamination and/or a subduction-related geochemical signatures is the Nb/Th ratio (Condie, 2003), with Nb/Th < 5 indicating crustal and or subduction contamination. All samples from

the Geita Greenstone Belt have Nb/Th > 5, with an average value of 8.32 (range 6.74–9.31) which is similar to the primitive mantle value of 8.39 (Sun and McDonough, 1989). Pearce (2008) used Th/Yb–Nb/Yb diagrams (Fig. 11a) as a proxy for crustal contamination, with crustally contaminated basalts plotting in oblique arrays above the modern MORB–OIB array. A subduction influence (e.g., arc proximity) may displace the composition of back arc basin basalts above the modern MORB–OIB array but preserve a sub-parallel trend. The Kiziba Formation metabasalts plot above the modern day MORB–OIB array having a sub-parallel trend, thus, suggesting some small degrees of Th enrichment or Nb depletion, which can be interpreted as addition of Th through a subduction component. The combined datasets (this study; Many, 2004; Many and Maboko, 2008), plot within and immediately above the modern day MORB–OIB array defining an overall oblique trend resembling crustal interaction vectors. We consider a subduction input highly unlikely and most probably the observed ratios reflect a non-depleted mantle source as suggested by near identical primitive mantle ratios (Fig. 11a), which are much lower than well-known back-arc basalts (no enrichment in Th over Nb when viewed in a primitive mantle normalized diagram) with a subduction component. On the other hand when plotted on a Nb/Y–Zr/Y diagram (Fig. 11b; Condie, 2005) the samples plot just below the primitive mantle and in a very restricted area, near primitive mantle composition, along a mixing array similar to that of other late Archean oceanic basalts, interpreted to represent a plume-head source (Condie, 2005). However, none of the samples plot towards an enriched mantle component or the subduction component. Thus, crustal and/or subduction-related contamination is unlikely.

9. A primitive mantle source for the Kiziba Formation metabasalts

Immobile and incompatible trace element ratios indicate little to no crustal or subduction related contamination of Kiziba Formation metabasalts, thus, most probably these ratios are a direct reflection of the mantle source. Most element ratios are similar to or identical to primitive mantle values suggesting a primitive mantle source. This is particularly obvious for Th/Nb (Fig. 10c; average = 0.12; PM = 0.12), Hf/Sm (average = 0.70; PM = 0.71); Sm/Nd (average = 0.32; PM = 0.33), Lu/Hf (average = 0.21; PM = 0.24) and Zr/Hf (average = 33.9; PM = 36). Note that ratios such as Th/Nb, Sm/Hf or Sm/Nd are less affected by the degree of melting compared to other incompatible trace element ratios and, therefore, they are good tracers of mantle source. On the other hand the Nb/Zr ratio is affected by the degree of partial melting; increased partial melting will lower the Nb/Zr ratio, which can explain the displacement from a primitive mantle composition towards a MORB like composition seen in Fig. 11b and d. Alternatively, the change in Nb/Zr ratio may indicate melting of a heterogeneous source involving depleted to primitive mantle.

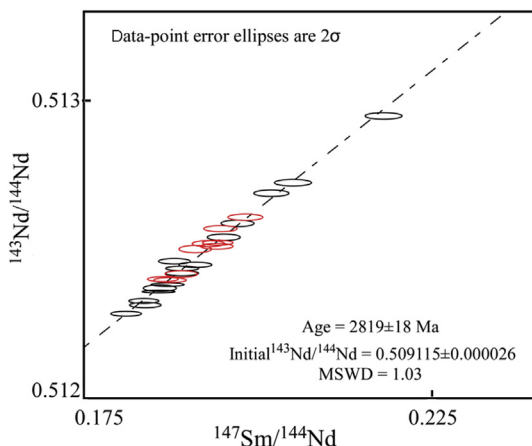


Figure 7. Diagram showing the whole rock Sm–Nd isochron for Kiziba Formation obtained by combining our dataset (red ellipses) with that of Many and Maboko (2008; black ellipses).

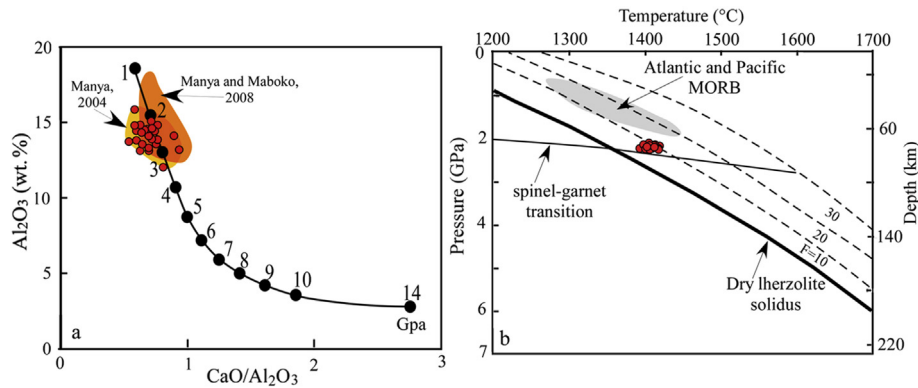


Figure 8. (a) Al₂O₃ versus CaO/Al₂O₃ (weight percent) diagram of Herzberg (1995) showing the pressure in GPa (numbers 1 to 14 represent the pressure in GPa) along the experimentally determined mantle solidus. The Kiziba Formation metabasalts plot between the 2 and 3 GPa interval suggesting a melting depth of 60–70 km. (b) Pressure – temperature diagram showing the temperature and melting depth for modern day MORB (data from Lee et al., 2009) and for Kiziba Formation metabasalts. The melting temperature for Kiziba Formation metabasalts was calculated using the method described in Till et al. (2012).

The Sm/Nd ratios vary between 0.30 and 0.37 with an average of 0.32, which are similar to the chondritic and primitive mantle values of 0.32 and 0.33 respectively (Fig. 12b; Sun and McDonough, 1989; McDonough and Sun, 1995; Lyubetskaya and Korenaga, 2007). These values are similar to those of Manya (2004) for the Rwamangaza area and Manya and Maboko (2008) for the eastern side of Geita Greenstone Belt. We can assume that these ratios are the minimum values of their source rock since any crustal contamination, will only lower these values. There is no correlation between the Mg[#] and Sm/Nd ratios, suggesting that the Sm/Nd ratio it is a source characteristic rather than a fractionation artefact. Moreover, similar ratios over a large area suggest a homogenous mantle source. All samples except one plot (Fig. 12b) below the depleted mantle Sm/Nd ratio (0.37) calculated by Salters and Stracke (2004) at 2800 Ma, thus indicating that the Kiziba Formation metabasalts have been extracted from a mantle source with a primitive mantle composition or from a mantle source that strongly interacted with and was modified by the primitive mantle.

The ϵ_{Nd} values (Fig. 12a) range between +2 and +2.9 while the ϵ_{Nd} value calculated from the isochron ($^{143}\text{Nd}/^{144}\text{Nd} = 0.509115$) is +2.2. The depleted mantle evolution line at 2800 Ma corresponds to $\epsilon_{\text{Nd}} = +3$ assuming a present day value of +8 or to $\epsilon_{\text{Nd}} = 4.8$ assuming a present day value of 12 (e.g., DePaolo and Wasserburg, 1976). A pure primitive mantle source model for the Kiziba Formation metabasalts implies a near chondritic ϵ_{Nd} value at 2800 Ma. The positive ϵ_{Nd} value may reflect the interaction of a deep primitive mantle source with the depleted upper mantle. However, the lack of any correlation between $^{143}\text{Nd}/^{144}\text{Nd}$ and Nd concentration indicates that the range in Nd isotope compositions is not related to a mixture of different sources, but rather a source characteristic related to parental magmas. The consistency of isotopic compositions over a large area (see also Manya and Maboko, 2003, 2008) further supports a uniform isotopic source for these metabasalts without any mixing or contamination.

10. Oceanic plateau basalts and plume head source

The general enrichment seen in the trace element geochemistry of the Kiziba Formation metabasalts causes them to plot just above the line separating plume from non-plume sources and within the field of the oceanic plateau basalts on the Nb/Y–Zr/Y diagram (Fig. 11b). The similarity of the geochemistry of the Kiziba Formation metabasalts to oceanic plateau basalts is further highlighted by their inferred derivation from a source having an incompatible trace

element composition similar to that of the primitive mantle. For example, geochemical modeling has shown that the Ontong Java Plateau basalts were generated by melting of primitive mantle (Fitton and Goddard, 2004; not depleted MORB) similar to the Kiziba Formation metabasalts. Other features characteristic of an oceanic plateau like environment include rapid eruption, restricted variation in composition over a large area and limited terrigenous input (e.g., Floyd, 1989; Sager, 2005; Benn and Moyen, 2008). The basalts in the Geita Greenstone Belt and in the Rwamangaza area to the south yield near identical eruption ages (~2822 Ma) that are within error, have a similar composition and contain little interbedded sediment.

Oceanic plateau basalts have been explained in terms of plume tectonics (e.g., Duncan and Richards, 1991; Condie, 2005; Kamber, 2015), with plume heads giving rise to basalts in the oceanic plateaus, or by decompression melting in the upper mantle, at plate edges or at zones of extension (e.g., Foulger, 2007). Many Archean basalt units with similar trace element geochemistry to the Kiziba Formation have been interpreted to be derived from plume sources (e.g., Condie, 2005). The early Archean (black double-headed arrow in Fig. 11b) and the late Archean (blue double headed arrow in Fig. 11b) oceanic plateau basalts or flood basalts that have been interpreted to be derived from plume sources plot along a mixing array between deep depleted mantle (DEP) and mantle with an enriched component (EN). The Kiziba Formation metabasalts plot (Fig. 11b) along the same mixing array as other late Archean basalts (blue double headed arrow in Fig. 11b), but no sample plots towards the deep depleted mantle (DEP) or towards the enriched mantle (EN). Therefore most probably their geochemistry reflects only the contribution of the plume head. The lack of any garnet signature (Fig. 9) in their trace element geochemistry further suggests a plume head source rather than derivation at greater depth.

11. Geodynamic setting during the late Archean in the Tanzania Craton

The geodynamic setting for the Archean Tanzania Craton has generally been interpreted in terms of a modern day plate tectonic scenario (e.g., Manya and Maboko, 2003; Manya, 2004; Cloutier et al., 2005; Manya et al., 2007; Manya and Maboko, 2008; Kabete et al., 2012) involving lateral terrane accretion and greenstone belt formation in back arc settings. The mafic volcanic rocks in the Sukumaland Greenstone Belt have been interpreted to represent a relatively homogenous sequence (based on trace element geochemistry and Nd isotopes) formed in a back-arc setting as a result of melting of a depleted mantle source that

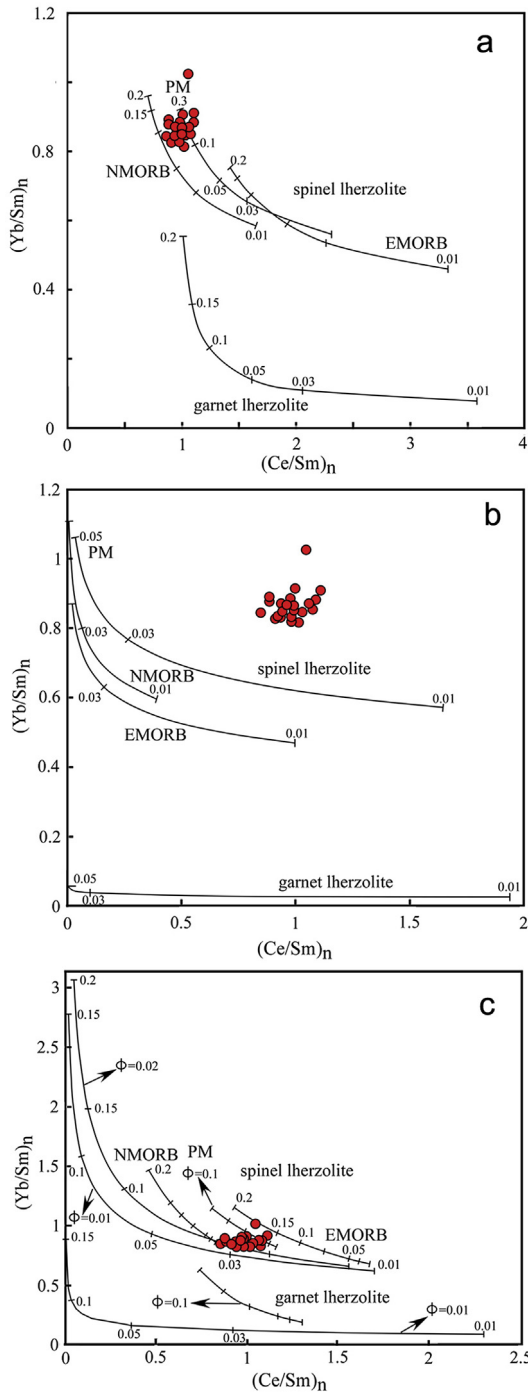


Figure 9. $(Yb/Sm)_n$ versus $(Ce/Sm)_n$ plots showing the effect of batch melting (a), fractional melting (b) and continuous melting (c) in the spinel peridotite field for rocks having EMORB, NMORB and PM (primitive mantle) mantle compositions. The numbers along the melting lines represent melt fractions. The trace element composition of the Kiziba Formation metabasalts is best explained by partial melting of a spinel-peridotite with a primitive mantle composition. The effect of partial melting of a garnet-lherzolite peridotite is also shown. The fact that all Kiziba Formation samples plot away from the garnet-lherzolite melting line and in a tight cluster along the spinel-lherzolite melting curve suggests that Kiziba Formation metabasalts were not contaminated by melts generated at great depth. The modal compositions used for modeling were, spinel-lherzolite (initial): olivine = 0.58; clinopyroxene = 0.12; orthopyroxene = 0.27; spinel = 0.033; spinel-lherzolite (melt): olivine = 0.1; clinopyroxene = 0.5; orthopyroxene = 0.27; spinel = 0.13; garnet-lherzolite (initial): olivine = 0.60; clinopyroxene = 0.076; orthopyroxene = 0.21; garnet = 0.115; garnet-lherzolite (melt): olivine = 0.05; clinopyroxene = 0.3; orthopyroxene = 0.2; garnet = 0.45. Mineral-melt partition coefficients are from White (2013).

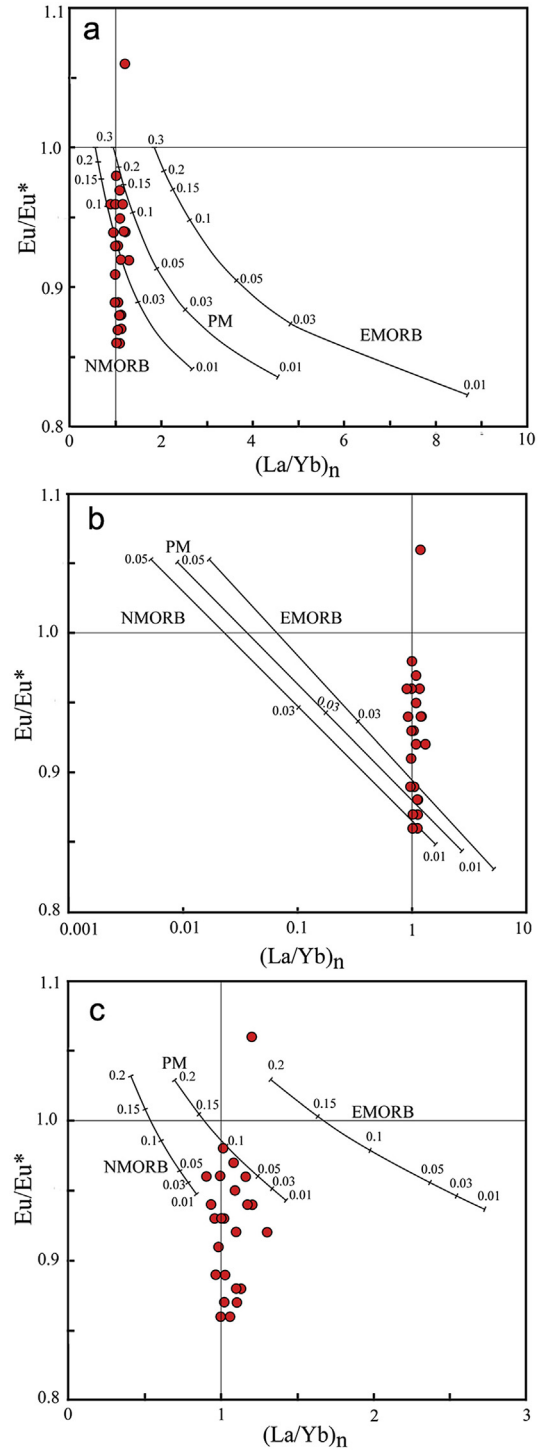


Figure 10. Eu/Eu^* versus $(La/Yb)_n$ diagrams showing the effect of different partial melting models, batch melting (a), fractional melting (b), continuous melting (c), on the Eu anomaly and the slope of the chondrite normalized REE pattern. The composition of the spinel-lherzolite and the partition coefficients are similar to the ones used in Fig. 9.

was metasomatised due to subduction related processes (e.g., Many and Maboko, 2003; Many, 2004; Cloutier et al., 2005; Many et al., 2007; Many and Maboko, 2008). To further strengthen their argument Many (2004) suggested that the 2780 ± 3 and 2808 ± 3 Ma felsic volcanism from the Kahama area (Fig. 1) was erupted in the same basin as the 2800 Ma mafic

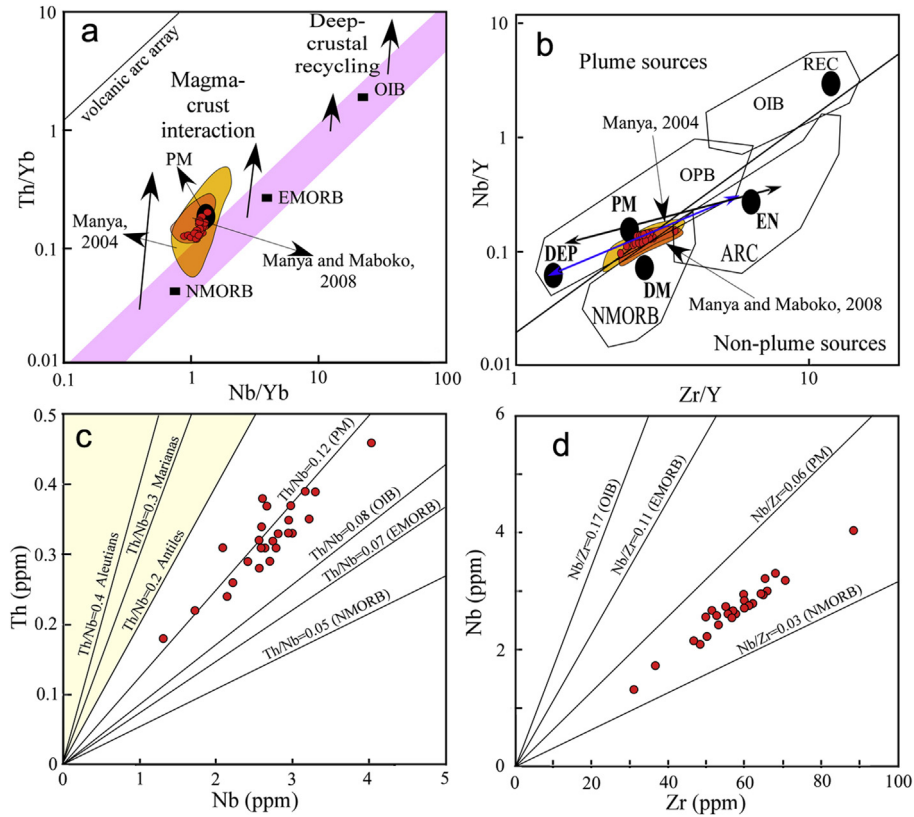


Figure 11. (a) Plot showing the distribution of Kiziba Formation metabasalts on a Th/Yb versus Nb/Yb diagram (Pearce, 2008), also showing the modern day compositional array for oceanic basalts and crustal contamination vectors. (b) Plot showing the distribution of Kiziba Formation metabasalts on the Nb/Y versus Zr/Y diagram (Condie, 2005). Blue arrow – a plume mixing array for late Archean non-arc basalts; black arrow – a plume mixing array for early Archean non-arc basalts (Condie, 2005). (c) Plot of Th versus Nb showing the distribution of Kiziba Formation metabasalts along the primitive mantle line of constant composition. Also plotted are minimum constant composition lines modern back arc basalts (data from Plank, 2005). (d) Plot of Nb versus Zr showing the displacement of the composition of basalt samples from the Kiziba Formation towards NMORB due the effect of partial melting. DEP – deep depleted mantle; PM – primitive mantle; DM – shallow depleted mantle; EN – enriched component; REC – recycled component; OPB – oceanic plateau basalt; OIB – ocean island basalt; ARC – arc related basalt; NMORB – normal ocean ridge basalt.

volcanics, thus inferring evidence for bimodal volcanism which is less typical for a subduction-type setting. On the other hand, the stratigraphic relationships in the Sukumaland Greenstone Belt and the Tanzania Craton in general are poorly understood (e.g., Many and Maboko, 2008; Sanislav et al., 2014), and relationship simple correlation between geographically widely dispersed units is not supported by the current field evidence (i.e. the high degree of

shearing and deformation that has affected the greenstone sequences). For example the felsic volcanics near Kahama are a few hundred kilometers away from the mafic volcanics from Tulawaka, Rwamangaza and Geita. The Sukumaland greenstone is highly fragmented by shear zones and by the intrusion of granites, and apart from a broad coincidence in age, there is no evidence that the supracrustal rocks in the Sukumaland Greenstone Belt formed in

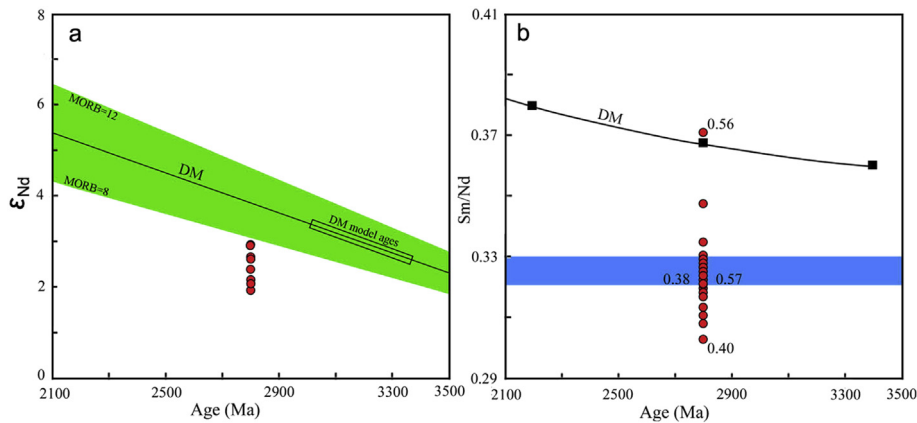


Figure 12. (a) Plot showing the variation in ϵ_{Nd} for the Kiziba Formation metabasalts at 2800 Ma. (b) Plot showing the variation in Sm/Nd ratio for the Kiziba Formation metabasalts and the calculated Sm/Nd ratios (values from Salters and Stracke, 2004) for depleted mantle in the late Archean. Note that the majority of Kiziba Formation plot near the primitive mantle values (blue stripe) (Sun and McDonough, 1989; Lyubetskaya and Korenaga, 2007).

the same basin or in adjacent basins. The Kiziba Formation metabasalts in the Geita Greenstone Belt are structurally bound and there is no direct evidence of synchronous felsic volcanism or sediment deposition in the Geita area. The metabasalts in the Rwamangaza area (e.g. [Manya and Maboko, 2003](#)) occur as float and isolated outcrops in younger granite and gneiss while the metabasalts near Tulawaka are not exposed (they have been sampled from drill core; [Cloutier et al., 2005](#)) and occur in association with much younger sediments and felsic volcanics. At Bulyanhulu ([Fig. 1](#)), mafic units occur with felsic volcanics and thin sedimentary horizons dominated by shale, with the mafic volcanics forming the base of the sequence, and shale units marking contacts with felsic volcanics/volcanoclastic rocks ([Chamberlain, 2003](#)). The Kiziba Formation mafic rocks represent the oldest unit in the entire Lake Victoria region with no basement rocks identified so far in the northern half of Tanzania Craton (e.g., [Manya and Maboko, 2008](#); [Sanislav et al., 2014](#)). The presence of extensive pillow structures is indicative of subaqueous eruption, which can take place in either an oceanic or continental setting. Thus the field relationships can alternatively be interpreted to indicate an oceanic plateau like setting. Modern oceanic plateaus, built on oceanic crust, such as Iceland and Ontong Java are dominated by mafic rocks but minor synchronous felsic volcanism is also present (e.g., [Sheth, 2007](#); [Martin et al., 2008](#); [Reimink et al., 2014](#)).

[Manya \(2004\)](#) and [Manya and Maboko \(2008\)](#) interpreted the trace element compositions of the basalt units in the Geita and Rwamangaza areas to indicate derivation from a heterogeneous mantle source, consisting of a mixture of depleted mantle, similar to present-day MORB source, and LREE-enriched and HFSE-depleted mantle source, similar to that feeding volcanism along modern convergent margins. Thus, the basalts have been interpreted to reflect an interaction of depleted mantle with melt derived from subduction of an oceanic slab in a back arc setting with this interpretation relying heavily on the overall flat REE patterns and small negative Nb anomalies. Similar age basalts from the Ramagiri-Hungund, Sigegudda and Jonnagiri greenstone belts of the Dharwar Craton (e.g., [Manikyamba et al., 2004, 2012 and 2014](#)) have a much more pronounced arc signature with strong Nb and Ti anomalies and depleted or enriched LREE patterns which, in contrast with the flat REE pattern of the Kiziba Formation basalts and the very small to missing Nb and Ti anomalies. Modern back arc basalts are known to have an arc signature in the initial stages of arc development and back arc opening, and transition into a typical MORB like signature in the more advanced stages (e.g., [Taylor and Martinez, 2003](#); [Pearce and Stern, 2006](#); [Bezos et al., 2009](#)). Taking these aspects into consideration, an advanced back arc setting as proposed by [Manya \(2004\)](#) and [Manya and Maboko \(2008\)](#) for the Kiziba Formation metabasalts cannot be disregarded. However, such an interpretation relies on the assumption that Kiziba Formation metabasalt has been extracted from a modern day like variably depleted mantle source with the observed enrichment attributed to subduction related metasomatism. We propose that the observed enrichment in the Kiziba Formation metabasalts is better explained as the result of extraction from a primitive mantle source, and/or different degree of partial melting of a primitive mantle source erupted in an oceanic plateau like setting.

12. Conclusions

This study has shown that the Kiziba Formation metabasalts occupy extensive areas in the Geita Greenstone Belt and add to previous observations (e.g., [Manya and Maboko, 2008](#); [Sanislav et al., 2014](#)) that the current stratigraphic division of the Sukumaland Greenstone Belt into an inner mafic-rich belt, and an outer felsic- and sediment-rich belt, is not valid, and the stratigraphy in

the Lake Victoria region of the Tanzania Craton will need to be revisited as more geochronological and geochemical data becomes available.

The Kiziba Formation metabasalts are the oldest rocks recognized so far in the northern part of the Tanzania Craton. The immobile and incompatible trace element ratios and Nd isotopes indicate that Kiziba Formation metabasalts were derived from partial melting of a primitive mantle source in the spinel peridotite stability field. Their geodynamic setting cannot be constrained by field relationships and the existing interpretation of a back arc setting for their genesis does not have strong support based on trace element geochemistry. Instead, the trace element and isotope geochemistry of the Kiziba Formation metabasalts are consistent with their formation in an environment similar to modern day oceanic plateaus, as a result of partial melting of a plume head that erupted through oceanic crust with little terrigenous input.

The Kiziba Formation metabasalts have a trace element composition indicative of source that was more enriched than the depleted mantle source of present-day MORB and closer to the composition of a more primitive mantle source and adds to previous studies (e.g., [Condie, 2005](#); [Kamber, 2015](#)), which indicate that Archean plumes or upper mantle was mostly primitive in composition, and therefore Archean ocean ridge basalts are difficult to recognize based on geochemistry alone. Alternatively, most Archean basalts were not generated along spreading centers similar to the modern mid-ocean ridges, but rather in an oceanic plateau like environment.

Acknowledgements

The authors would like to acknowledge funding and the access to information provided by Geita Gold Mine and AngloGold Ashanti. Sergio Kolling and Steve Robins are particularly acknowledged for their continuous support during the duration of this study. The staff and the superb analytical facilities at the Advanced Analytical Centre hosted by James Cook University have made this work much easier. We would like to acknowledge Julian Pearce for reading and early version of the manuscript and for providing very useful comments. In depth reviews by Marlina Elburg and an anonymous reviewer are greatly appreciated.

Appendix A. Supplementary data

Supplementary data related to this article can be found at <http://dx.doi.org/10.1016/j.gsf.2015.11.008>.

References

- [Arndt, N.T., 2003.](#) Komatiites, kimberlites and boninites. *Journal of Geophysical Research* 108 (B6), 2293.
- [Arndt, N.T., Nesbitt, R.W., 1982.](#) Geochemistry of Munro Township basalts. In: [Arndt, N.T., Nisbet, E.G. \(Eds.\), Komatiites.](#) Allen and Unwin, Concord, Mass, pp. 309–330.
- [Arndt, N.T., Kerr, A.C., Tarney, J., 1997.](#) Dynamic melting in plume heads: the formation of Gorgona komatiites and basalts. *Earth and Planetary Science Letters* 146, 289–301.
- [Barth, H., 1990.](#) Provisional geological map of the Lake Victoria gold fields Tanzania 1:500,000 (with explanatory notes). *Geologisches Jahrbuch* 72, 3–59.
- [Bédard, J.H., Harris, L.B., Thurston, P., 2014.](#) The hunting of the snArc. *Precambrian Research* 229, 20–48.
- [Benn, K., Moyen, J.-F., 2008.](#) The late Archean Abitibi-Opatoca terrane, Superior Province: a modified oceanic plateau. In: [Condie, K.C., Pease, V. \(Eds.\), When Did Plate Tectonics Begin on Planet Earth?](#) Geological Society of America Special Paper 440, pp. 173–197.
- [Bezos, A., Escrig, S., Langmuir, C.H., Michael, P.J., Asimow, P.D., 2009.](#) Origins of chemical diversity of back-arc basin basalts: a segment-scale study of the Eastern Lau spreading center. *Journal of Geophysical Research* 114, B06212.
- [Bolhar, R., Woodhead, J.D., Hergt, J.M., 2003.](#) Continental setting inferred for emplacement of the 2.9–2.7 Ga Belingwe Greenstone Belt, Zimbabwe. *Geology* 31, 295–298.

- Borg, G., 1992. New aspects on the lithostratigraphy and evolution of the Siga Hills, an Archaean granite-greenstone terrain in NW-Tanzania. *Zeitschrift für Angewandte Geologie* 38 (2), 89–93.
- Borg, G., Krogh, T., 1999. Isotopic age data of single zircons from the Archaean Sukumaland Greenstone Belt, Tanzania. *Journal of African Earth Sciences* 29, 301–312.
- Borg, G., Shackleton, R.M., 1997. The Tanzania and NE Zaire Cratons. In: de Wit, M.J., Ashwal, L.D. (Eds.), *Greenstone Belts*. Clarendon Press, Oxford, pp. 608–619.
- Chamberlain, C.M., 2003. *Geology and Genesis of Gold Mineralization at the Bulyanhulu Gold Deposit, Sukumaland Greenstone Belt, Tanzania*. Ph.D. Thesis. Imperial College, University of London, London, 401pp.
- Chamberlain, C.M., Tosdal, R.M., 2007. U–Pb Geochronology of the Lake Victoria Greenstone Terrane, Tanzania. Mineral Deposit Research Unit The University of British Columbia (Research Program on World-class Gold Deposits and Advanced Exploration Projects Owned and/or Joint Ventured to Barick Gold, Placer Dome, Anglo-Gold Ashanti, Resolute Mining NL as Main Sponsors.
- Chardon, D., Choukroune, P., Jayananda, M., 1996. Strain patterns, decollement and incipient sagducted greenstone terrains in the Archaean Dharwar craton (South India). *Journal of Structural Geology* 18, 991–1004.
- Chardon, D., Choukroune, P., Jayananda, M., 1998. Sinking of the Dharwar Basin (South India): implications for Archaean tectonics. *Precambrian Research* 91 (1–2), 15–39.
- Choukroune, P., Bouhallier, H., Arndt, N.T., 1995. Soft lithosphere during periods of Archaean crustal growth or crustal reworking. In: Coward, M.P., Ries, A.C. (Eds.), *Early Precambrian Processes*. Geological Society, London, Special Publications 95, pp. 67–86.
- Clifford, T.N., 1970. *The structural framework of Africa*. Oliver and Boyd Edinburgh 1–26.
- Cloutier, J., Stevenson, R.K., Bardoux, M., 2005. Nd isotopic, petrologic and geochemical investigation of the Tulawaka East gold deposit, Tanzania Craton. *Precambrian Research* 139, 147–163.
- Condie, K.C., 2003. Incompatible element ratios in oceanic basalts and komatiites: tracking deep mantle sources and continental growth rates with time. *Geochemistry, Geophysics, Geosystems* 4 (1), 1–28.
- Condie, K.C., 2005. High field strength element ratios in Archean basalts: a window to evolving sources of mantle plumes? *Lithos* 79, 491–504.
- Cutts, K.A., Stevens, G., Hoffmann, E.J., Buick, I.S., Frei, D., Münker, C., 2014. Paleo- to Mesoarchean polymetamorphism in the Barberton Granite-Greenstone Belt, South Africa: constraints from U–Pb monazite and Lu–Hf garnet geochronology on the tectonic processes that shaped the belt. *Geological Society of America Bulletin* 126 (3–4), 251–270.
- DePaolo, D.J., Wasserburg, G.J., 1976. Inferences about magma sources and mantle structure from variations of $^{143}\text{Nd}/^{144}\text{Nd}$. *Geophysical Research Letters* 3, 743–746.
- Duncan, R.A., Richards, M.A., 1991. Hotspots, mantle plumes, flood basalts, and true polar wander. *Reviews of Geophysics* 29, 31–50.
- Fawley, A.P., 1951. Preliminary Report on the Geita Gold Mining Company Limited Tanganyika. Rep AF/5, Geological Survey Tanganyika, File Number C 1120, Dodoma.
- Fitton, J.G., Goddard, M., 2004. Origin and evolution of magmas on the Ontong Java Plateau. In: Fitton, J.G., et al. (Eds.), *Origin and Evolution of the Ontong Java Plateau*. Geological Society, London, Special Publications 229, pp. 239–257.
- Floyd, P.A., 1989. Geochemical features of intraoceanic plateau basalts. In: Saunders, A.D., Norry, M.J. (Eds.), *Magmatism in the Ocean Basins*. Geological Society, London, Special Publications 42, pp. 215–230.
- Fouler, G.R., 2007. The “plate” model for the genesis of melting anomalies. In: Fouler, G.R., Jurdy, D.M. (Eds.), *Plates, Plumes, and Planetary Processes*, Geological Society of America Special Papers 430, pp. 1–28.
- Green, M.G., Sylvester, P.J., Buick, R., 2000. Growth and recycling of early Archaean continental crust: geochemical evidence from the Coonterunah and Warrawoona Groups, Pilbara Craton, Australia. *Tectonophysics* 322, 69–88.
- Herzberg, C., 1995. Generation of plume magmas through time: an experimental approach. *Chemical Geology* 126, 1–16.
- Herzberg, C., Asimow, P.D., 2008. Petrology of some oceanic island basalts: PRIMELT2.XLS software for primary magma calculation. *Geochemistry, Geophysics, Geosystems* 9, Q09001.
- Hofmann, A.W., 2003. Sampling mantle heterogeneity through oceanic basalts: isotopes and trace elements. In: Carlson, R.W. (Ed.), *Treatise on Geochemistry*. Elsevier, pp. 61–101.
- Hofmann, A., Dirks, P.H.G.M., Jelsma, H.A., 2001a. Horizontal tectonic deformation geometries in a late Archaean sedimentary sequence, Belingwe greenstone belt, Zimbabwe. *Tectonics* 20, 909–932.
- Hofmann, A., Dirks, P.H.G.M., Jelsma, H.A., 2001b. Late Archaean foreland basin deposits, Belingwe greenstone belt, Zimbabwe. *Sedimentary Geology* 141–142, 131–168.
- Hofmann, A., Dirks, P.H.G.M., Jelsma, H.A., Matura, N., 2003. A tectonic origin for ironstone horizons in the Zimbabwe craton and their significance for greenstone belt geology. *Journal of the Geological Society of London* 160, 83–97.
- Hollings, P., Kerrich, R., 1999. Trace element systematics of ultramafic and mafic volcanic rocks from the 3 Ga North Caribou greenstone belt, northwestern Superior Province. *Precambrian Research* 93, 257–279.
- Hollings, P., Wyman, D.A., Kerrich, R., 1999. Komatiite – basalt – rhyolite volcanic associations in northern Superior Province greenstone belts: significance of plume-arc interaction in the generation of the proto-continental Superior Province. *Lithos* 46, 137–161.
- Hunter, M.A., Bickle, M.J., Nisbet, E.G., Martin, A., Chapman, H.J., 1998. Continental extensional setting for the Archaean Belingwe Greenstone Belt, Zimbabwe. *Geology* 26, 883–886.
- Iwamori, H., Nakamura, H., 2015. Isotopic heterogeneity of oceanic, arc and continental basalts and its implications for mantle dynamics. *Gondwana Research* 27 (3), 1131–1152.
- Jayananda, M., Peucat, J.J., Chardon, D., Krishna Rao, B., Fanning, C.M., Corfu, F., 2013. Neoproterozoic greenstone volcanism and continental growth, Dharwar craton, southern India: constraints from SIMS U–Pb zircon geochronology and Nd isotopes. *Precambrian Research* 227, 55–76.
- Jelsma, H.A., Dirks, P.H.G.M., 2002. Neoproterozoic tectonic evolution of the Zimbabwe Craton. In: Fowler, C.M.R., Ebinger, C., Hawkesworth, C.J. (Eds.), *The Early Earth: Physical, Chemical and Biological Development*, Geological Society of London Special Publication 199, pp. 183–211.
- Jochum, K.P., Arndt, N.T., Hoffman, A.W., 1991. Nb–Th–La in komatiites and basalts: constraints on komatiites petrogenesis and mantle evolution. *Earth and Planetary Science Letters* 107, 272–289.
- Jochum, K.P., Stoll, B., Herwig, K., et al., 2006. MPI-DING reference glasses for in situ microanalysis: new reference values for element concentrations and isotope ratios. *Geochemistry, Geophysics, Geosystems* 7, Q02008. <http://dx.doi.org/10.1029/2005GC001060>.
- Kabete, J.M., Groves, D.L., McNaughton, N.J., Mruma, A.H., 2012. A new tectonic and temporal framework for the Tanzanian Shield: implications for gold metallogeny and undiscovered endowment. *Ore Geology Reviews* 48, 88–124.
- Kamber, B.S., 2015. The evolving nature of terrestrial crust from the Hadean, through the Archaean, into the Proterozoic. *Precambrian Research* 258, 48–82.
- Kerr, A.C., Mahoney, J.J., 2007. Oceanic plateaus: problematic plumes, potential paradigms. *Chemical Geology* 241, 332–353.
- Kerrich, R., Xie, Q., 2002. Compositional recycling structure of an Archaean superplume: Nb–Th–U–REE systematics of Archaean komatiites and basalts revisited. *Contributions to Mineralogy and Petrology* 142, 476–484.
- Kerrich, R., Wyman, D., Hollings, P., Polat, A., 1999. Variability of Nb/U and Th/La in 3.0 to 2.7 Ga Superior Province ocean plateau basalts: application for the timing of continental growth and lithosphere recycling. *Earth and Planetary Science Letters* 168, 101–115.
- Korenaga, J., 2006. Archaean geodynamics and the thermal evolution of Earth. In: Benn, K., Mareschal, J.-C., Condie, K. (Eds.), *Archaean Geodynamics and Environments*, Geophysical Monograph Series, vol. 164. AGU, Washington DC, pp. 7–32.
- Korenaga, J., 2013. Initiation and evolution of plate tectonics on Earth: theories and observations. *Annual Review of Earth and Planetary Sciences* 41, 117–151.
- Kuehn, S., Ogola, J., Sango, P., 1990. Regional setting and nature of gold mineralization in Tanzania and southwest Kenya. *Precambrian Research* 46, 71–82.
- Kusky, T.M. (Ed.), 2004. *Precambrian Ophiolites and Related Rocks*. Elsevier, Amsterdam, 748 pp.
- Kusky, T.M., Kidd, W.S.F., 1992. Remnants of an Archean oceanic plateau, Belingwe Greenstone Belt, Zimbabwe. *Geology* 20, 43–46.
- Kusky, T.M., Winsky, P.A., 1995. Structural relationships along a greenstone/shallow water shelf contact, Belingwe Greenstone Belt, Zimbabwe. *Tectonics* 14, 448–471.
- Lafliche, M.R., Dupuy, C., Bougault, H., 1992. Geochemistry and petrogenesis of Archean mafic volcanic rocks of the southern Abitibi belt, Quebec. *Precambrian Research* 57, 207–241.
- Lee, C.-T., Luffi, P., Plank, T., Dalton, H., Leeman, W.P., 2009. Constraints on the depths and temperatures of basaltic magma generation on Earth and other terrestrial planets using new thermobarometers for mafic magmas. *Earth and Planetary Science Letters* 279, 20–33.
- Lyubetskaya, T., Korenaga, J., 2007. Chemical composition of the Earth primitive mantle and its variance: 1. Method and results. *Journal Geophysical Research* 112, B03211.
- Manikyamba, C., Kerrich, R., Naqvi, S.M., Ram Mohan, M., 2004. Geochemical systematics of tholeiitic basalts from the 2.7 Ga Ramagiri–Hungund composite greenstone belt, Dharwar craton. *Precambrian Research* 134, 21–39.
- Manikyamba, C., Kerrich, R., Polat, A., Raju, K., Satyanarayanan, M., Krishna, A.K., 2012. Arc picrite–potassic adakitic–shoshonitic volcanic association of the Neoproterozoic Sigegudda Greenstone Terrane, Western Dharwar Craton: transition from arc Wedge to lithosphere melting. *Precambrian Research* 212–213, 207–224.
- Manikyamba, C., Ganguly, S., Santosh, M., Rajanikanta Singh, M., Saha, A., 2014. Arc-nascent back arc signature in metabasalts from the Neoproterozoic Jonnagiri greenstone terrane, Eastern Dharwar Craton, India. *Geological Journal* 50, 651–669.
- Manya, S., 2004. Geochemistry and petrogenesis of volcanic rocks of the Neoproterozoic Sukumaland greenstone belt, northwestern Tanzania. *Journal of African Earth Sciences* 40, 269–279.
- Manya, S., 2012. Mg-rich metabasalts from the southern Musoma–Mara greenstone belt: possible evidence for mantle plume activity in the Tanzania craton? *Tanzania Journal of Science* 38, 71–84.
- Manya, S., Maboko, M.A.H., 2003. Dating basaltic volcanism in the Neoproterozoic Sukumaland Greenstone Belt of the Tanzania Craton using the Sm–Nd method: implications for the geological evolution of the Tanzania Craton. *Precambrian Research* 121, 35–45.
- Manya, S., Maboko, M.A.H., 2008. Geochemistry of the Neoproterozoic mafic volcanic rocks of the Geita area, NW Tanzania: implications for stratigraphical relationships in the Sukumaland greenstone belt. *Journal of African Earth Sciences* 52, 152–160.

- Manya, S., Maboko, M.A.H., Nakamura, E., 2007. The geochemistry of high-Mg andesite and associated adakitic rocks in the Musoma-Mara Greenstone Belt, northern Tanzania: possible evidence for Neoproterozoic ridge subduction? *Precambrian Research* 159, 241–259.
- Martin, E., Martin, H., Sigmarrsson, O., 2008. Could Iceland be a modern analogue for the Earth's early continental crust? *Terra Nova* 20, 463–468.
- McDonough, W.F., Sun, S.-S., 1995. Composition of the Earth. *Chemical Geology* 120, 223–253.
- Messo, C., Manya, S., Maboko, M.A.H., 2012. Geochemistry of the Neoproterozoic volcanic rocks of the Kilimafedha greenstone belt, Northeastern Tanzania. *Journal of Geological Research* 1–18.
- Mtoro, M., Maboko, M.A.H., Manya, S., 2009. Geochemistry and geochronology of the bimodal volcanic rocks of the Suguti area in the southern part of the Musoma-Mara Greenstone Belt, Northern Tanzania. *Precambrian Research* 174, 241–257.
- Myers, J.S., 2001. Protoliths of the 3.8–3.7 Ga Isua greenstone belt, west Greenland. *Precambrian Research* 105, 129–141.
- Naqvi, S.M., Ram Mohan, M., Rana Pratap, J.G., Srinivasa Sarma, D., 2009. Adakite-TTG connection and fate of Mesoproterozoic basaltic crust of Hole-narsipur Nucleus, Dharwar Craton, India. *Journal of Asian Earth Sciences* 35, 416–434.
- O'Neil, J., Carlson, R.W., Paquette, J.L., Francis, D., 2013. Formation age and metamorphic history of the Nuvvuagittuq Greenstone Belt. *Precambrian Research* 220–221, 23–44.
- Ohtani, E., Kawabe, I., Moriyama, J., Nagata, Y., 1989. Partitioning of elements between majorite garnet and melt and implications for petrogenesis of komatiites. *Contributions to Mineralogy and Petrology* 103, 263–269.
- Parman, S.W., Grove, T.L., Dann, J.C., 2001. The production of Barberton komatiites in an Archean subduction zone. *Geophysical Research Letters* 28, 2513–2516.
- Pearce, J.A., 2008. Geochemical fingerprinting of oceanic basalts with applications to ophiolite classification and the search for Archean oceanic crust. *Lithos* 100, 14–48.
- Pearce, J.A., Stern, R.J., 2006. The origin of back-arc basin magmas: trace element and isotope perspectives. In: Christie, D.M., et al. (Eds.), *Back-arc Spreading Systems: Geological, Biological, Chemical and Physical Interactions*, Geophysical Monograph, vol. 166. AGU, Washington, D.C., pp. 63–86.
- Percival, J.A., Sanborn-Barrie, M., Skulski, T., Stott, G.M., Helmstaedt, H., White, D.J., 2006. Tectonic evolution of the western Superior Province from NATMAP and Lithoprobe studies. *Canadian Journal of Earth Science* 43, 1085–1117.
- Percival, J., Skulski, T., Sanborn-Barrie, M., Stott, G., Leclair, A.D., Corkery, M.T., Boily, M., 2012. Geology and tectonic evolution of the Superior Province, Canada. In: Percival, J., Cook, F., Clowes, R. (Eds.), *Tectonic Styles in Canada: The Lithoprobe Perspective*. Geological Association of Canada, Special Paper, St John's, NF, Canada, vol. 49, pp. 321–378.
- Pettke, 2008. Analytical protocols for element concentration and isotope ratio measurements in fluid inclusions by LA-(MC)-ICP-MS. In: Sylvester, P. (Ed.), *Laser Ablation ICP-MS in the Earth Sciences: Current Practices and Outstanding Issues*, Short Course Series 40. Mineralogical Association of Canada, Vancouver, pp. 189–212.
- Plank, T., 2005. Constraints from Thorium/Lanthanum on sediment recycling at subduction zones and the evolution of the continents. *Journal of Petrology* 46, 921–944.
- Polat, A.R., Kerrich, R., 2000. Archean greenstone belt magmatism and the continental growth-mantle evolution connection: constraints from Th–U–Nb–LREE systematics of the 2.7 Ga Wawa subprovince, Superior Province, Canada. *Earth and Planetary Science Letters* 175, 41–54.
- Polat, A., Hofmann, A.W., Rosing, M.T., 2002. Boninite-like volcanic rocks in the 3.7–3.8 Ga Isua greenstone belt, West Greenland: geochemical evidence for intra-oceanic subduction zone processes in the early Earth. *Chemical Geology* 184, 231–254.
- Puchtel, I.S., Hofmann, A.W., Amelin, Y.V., et al., 1999. Combined mantle plume-island arc model for the formation of the 2.9 Ga Sumzero-Kenozero greenstone belt, SE Baltic Shield: Isotope and trace element constraints. *Geochimica et Cosmochimica Acta* 63, 3579–3595.
- Quennell, A.M., McKinley, A.C.M., Aiken, W.G., 1956. Summary of the geology of Tanganyika: introduction and stratigraphy. Tanganyika Geological Survey Memoir 1 (pt 1), 264.
- Reimink, J.R., Chacko, T., Stern, R.A., Heaman, L.M., 2014. Earth's earliest evolved crust generated in an Iceland-like setting. *Nature Geoscience* 7, 529–533.
- Sager, W.W., 2005. What built Shatsky Rise, a mantle plume or ridge tectonics? In: Foulger, G.R., et al. (Eds.), *Plates, Plumes, and Paradigms*. Geological Society of America Special Papers 388, pp. 721–733.
- Salter, V.J.M., Stracke, A., 2004. The composition of the depleted mantle. *Geochemistry, Geophysics, Geosystems* 5, Q05B07.
- Sanislav, I.V., Wormald, R.J., Dirks, P.H.G.M., Blenkinsop, T.G., Salamba, L., Joseph, D., 2014. Zircon U–Pb ages and Lu–Hf isotope systematics from late-tectonic granites, Geita greenstone belt: implications for crustal growth of the Tanzania craton. *Precambrian Research* 242, 187–204.
- Sheth, H., 2007. Large Igneous Provinces (LIPs): definition, recommended terminology, and a hierarchical classification. *Earth Science Reviews* 85, 117–124.
- Shimizu, K., Nakamura, E., Maruyama, S., 2005. The geochemistry of ultramafic to mafic volcanics from the Belingwe Greenstone Belt, Zimbabwe: magmatism in an Archean Continental Large Igneous Province. *Journal of Petrology* 46, 2367–2394.
- Spandler, C., Pettke, T., Rubatto, D., 2011. Internal and external fluid sources for eclogite-facies veins in the Monviso meta-ophiolite, Western Alps: implications for fluid flow in subduction zones. *Journal of Petrology* 52, 1207–1236.
- Stott, G., Mueller, W., 2009. Superior Province: the nature and evolution of the Archean continental lithosphere. *Precambrian Research* 168, 1–3.
- Sun, S.-S., McDonough, W.F., 1989. Chemical and isotopic systematics of oceanic basalts: implications for mantle composition and processes. In: Saunders, A.D., Norry, M.J. (Eds.), *Magmatism in the Ocean Basins*. Geological Society, London, Special Publications, pp. 313–345.
- Taylor, B., Martinez, F., 2003. Back-arc basin basalt systematics. *Earth and Planetary Science Letters* 210, 481–497.
- Till, C.B., Grove, T.L., Krawczynski, M.J., 2012. A melting model for variably depleted and enriched lherzolite in the plagioclase and spinel stability fields. *Journal of Geophysical Research: Solid Earth* 117, B06206. <http://dx.doi.org/10.1029/2011JB009044>.
- van Acherbergh, E., Ryan, C.G., Jackson, S.E., Griffin, W.L., 2001. Data reduction software for LA-ICP-MS. In: Sylvester, P. (Ed.), *Laser-ablation-ICPMS in the Earth Sciences: Principles and Applications*, Short Course 29. Mineralogical Association of Canada, pp. 239–243.
- Van Hunen, J., Moyen, J.F., 2012. Archean subduction: fact or fiction? *Annual Review of Earth and Planetary Sciences* 40, 195–219.
- White, W.M., 2013. *Geochemistry*. Wiley-Blackwell, 668pp.
- Williams, H.M., Bizimis, M., 2014. Iron isotope tracing of mantle heterogeneity within the source regions of oceanic basalts. *Earth and Planetary Science Letters* 404, 396–407.
- Wirth, K.R., Vervoot, J.D., Weisberger, B., 2004. Origin and evolution of the Kilimafedha greenstone belt, eastern Tanzania Craton: evidence from Pb isotopes. *Geological Society of America Abstracts with Programs* 36, 244.